Finite Elements in Analysis and Design 236 (2024) 104155

Contents lists available at ScienceDirect

Finite Elements in Analysis & Design

journal homepage: www.elsevier.com/locate/finel

Polytopal templates for semi-continuous vectorial finite elements of arbitrary order on triangulations and tetrahedralizations

Adam Sky *, Ingo Muench

Institute of Structural Mechanics, Statics and Dynamics, Technische Universität Dortmund, August-Schmidt-Str. 8, 44227 Dortmund, Germany

ARTICLE INFO

Keywords:
Polytopal templates
Nédélec elements
Brezzi–Douglas–Marini elements
Raviart–Thomas elements
Piola transformations
Relaxed micromorphic model

ABSTRACT

The Hilbert spaces $H(\mathrm{curl})$ and $H(\mathrm{div})$ are employed in various variational problems formulated in the context of the de Rham complex in order to guarantee well-posedness. Seeing as the well-posedness follows automatically from the continuous setting to the discrete setting in the presence of commuting interpolants as per Fortin's criterion, the construction of conforming subspaces becomes a crucial step in the formulation of stable numerical schemes. This work aims to introduce a novel, simple method of directly constructing semi-continuous vectorial base functions on the reference element via template vectors associated with the geometric polytopes of the element and an underlying H^1-conforming polynomial subspace. The base functions are then mapped from the reference element to the element in the physical domain via consistent Piola transformations. The method is defined in such a way, that the underlying H^1-conforming subspace can be chosen independently, thus allowing for constructions of arbitrary polynomial order. We prove a linearly independent construction of Nédélec elements of the first and second type, Brezzi–Douglas–Marini elements, and Raviart–Thomas elements on triangulations and tetrahedralizations. The application of the method is demonstrated with two examples in the relaxed micromorphic model.

1. Introduction

In many variational problems well-posedness necessitates the employment of either the $H(\mathrm{curl})$ or $H(\mathrm{div})$ Hilbert spaces. Some classical examples are Maxwell's equations [1–3], Stokes-Darcy flows [4–6] and mixed Laplace problems [7,8]. More recent examples are the tangential-displacement-normal-normal-stress (TDNNS) method in elasticity [9,10], and the relaxed micromorphic model [11–13]. Other examples are curl based plasticity models [14,15]. Commonly, the application of the $H(\mathrm{curl})$ or $H(\mathrm{div})$ spaces arises in problems associated with the de Rham complex [16,17]. In fact, as shown in [18], complexes are a powerful and general tool for mixed variational formulations. The latter is also demonstrated in [19–22] where the elasticity complex and the $\mathrm{div}\,\mathrm{Div}$-complex are explored in the context of mixed formulations of linear elasticity and the biharmonic equation, respectively. Unlike in the classical Hilbert space H^1, an element of the $H(\mathrm{curl})$-space is only required to be tangentially continuous [23]. Analogously, elements of the $H(\mathrm{div})$-space are only required to be normal-continuous [23]. As such, the formulation of $H(\mathrm{curl})$- and $H(\mathrm{div})$-conforming finite elements is more complex, seeing as the continuity of the elements is required to be between C^0-continuous and discontinuous. The pioneering works [24,25] introduced the Nédélec elements of the first and second types, which represent polynomial subspaces with the minimal regularity requirements of the $H(\mathrm{curl})$-space $\mathcal{N}_{II}^p \subset \mathcal{N}_I^p \subset H(\mathrm{curl})$. In [26,27] the authors

* Corresponding author.
E-mail addresses: adam.sky@tu-dortmund.de (A. Sky), ingo.muench@tu-dortmund.de (I. Muench).

https://doi.org/10.1016/j.finel.2024.104155
Received 29 November 2023; Received in revised form 19 February 2024; Accepted 17 March 2024
Available online 26 March 2024
0168-874X/© 2024 The Authors. Published by Elsevier B.V. This is an open access article under the CC BY license (http://creativecommons.org/licenses/by/4.0/).

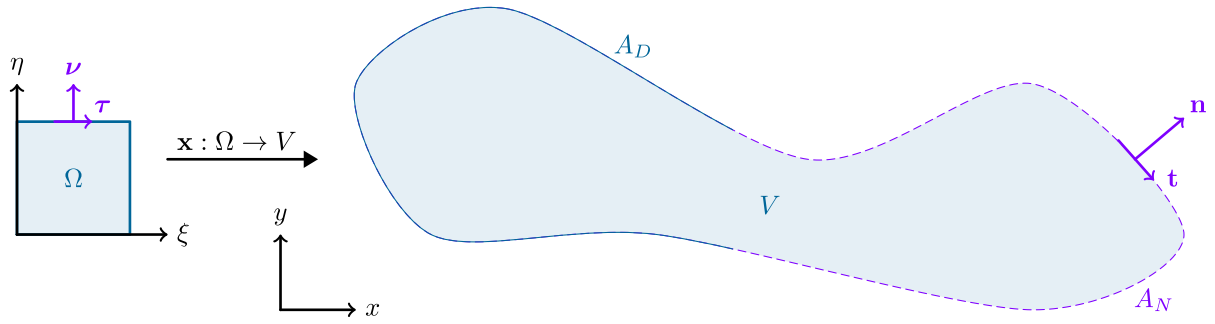

Fig. 1. A domain V with Dirichlet and Neumann boundaries mapped from some reference domain Ω.

introduced the Brezzi–Douglas–Marini and Raviart–Thomas elements, that allow to construct polynomial subspaces for the $H(\mathrm{div})$-space $\mathcal{BDM}^p \subset \mathcal{RT}^p \subset H(\mathrm{div})$, such that the elements exhibit the minimal regularity needed in $H(\mathrm{div})$. The elements are given in the classical element definition as per Ciarlet [28], and allow for application on general grids.

An alternative methodology to construction of a basis directly on the grid is to build base functions on the reference elements and map them to the physical elements on the grid by consistent transformations. The construction of low order vectorial finite elements is demonstrated in [29–33]. The formulation of higher order elements on the basis of Legendre polynomials can be found in [23,34,35]. Further, in [36,37], the authors present a higher order construction based on Bernstein polynomials. We note that in general, the mapping alone does not suffice in order to assert a consistent transformation and some additional algorithmic is required in order to avoid the so called orientation problem [29–31,34,38,39] (see Appendix B for the solution we use in this work).

The aim of this work is to establish a method of defining $H(\mathrm{curl})$ and $H(\mathrm{div})$ base functions on the reference element, **such that the underlying polynomial basis can be chosen independently**. As such, the method allows to directly construct conforming finite elements by using for example, Lagrange, Legendre [35], Jacobi [34] or Bernstein [40] polynomials. In conjunction with a hierarchical basis such as presented in [41], the construction automatically allows for anisotropic p-refinement. This goal is achieved by defining a template on the reference element, which can be subsequently used in conjunction with an H^1-conforming polynomial basis of one's choice, in order to span a semi-continuous finite element space. The template is composed of vector sets associated with the polytopes of the reference element, **where "polytope" is a general term for one of the geometric building blocks of the element domain: vertex, edge, face, or the cell**. Consequently, we dub the methodology "polytopal templates". In this work we consider subspaces for the Hilbert spaces $H(\mathrm{curl})$ and $H(\mathrm{div})$ on triangular and tetrahedral elements. For simplicity, we only consider real numbers, and do not discuss complex-valued base functions in this work. We mention that a related concept has been proposed in [42] for Nédélec type two and Brezzi–Douglas–Marini triangular elements **directly on the physical grid**. In contrast, this work introduces the construction on the reference element and applies consistent transformations.

This paper is structured as follows. First, we introduce the classical Hilbert spaces and their corresponding differential and trace operators. Next, we derive two-dimensional polytopal templates for the construction of Nédélec elements of the first and second type, Brezzi–Douglas–Marini elements, and Raviart–Thomas elements on the reference triangle. The methodology is subsequently utilized to derive polytopal templates on the reference tetrahedron for Nédélec elements of the second type and Brezzi–Douglas–Marini elements. We demonstrate the application of elements using the relaxed micromorphic model [11,30,31,43] with one example in antiplane shear and one three-dimensional example. Lastly, we present our conclusions and outlook.

The following definitions are employed throughout this work, see also Fig. 1:

- Vectors are indicated by bold letters. Non-bold letters represent scalars.
- In general, formulas are defined using the Cartesian basis, where the base vectors are denoted by $\mathbf{e}_1$, $\mathbf{e}_2$ and $\mathbf{e}_3$.
- Three-dimensional domains in the physical space are denoted with $V \subset \mathbb{R}^3$. The corresponding reference domain is given by Ω.
- Analogously, in two dimensions we employ $A \subset \mathbb{R}^2$ for the physical domain and Γ for the reference domain.
- Curves on the physical domain are denoted by s, whereas curves in the reference domain by μ.
- The tangent and normal vectors in the physical domain are given by $\mathbf{t}$ and $\mathbf{n}$, respectively. Their counterparts in the reference domain are $\boldsymbol{\tau}$ for tangent vectors and $\boldsymbol{\nu}$ for normal vectors.
- The polytopes of an element are identified using multi-indices. For example, edge e_j with $j = (1,2) \in \mathcal{J} = \{(1,2),(2,3),\dots\}$, where $\{1,2,3,\dots\}$ are the indices of the vertices $\{v_1, v_2, v_3\}$.
- In our construction of finite element spaces we use tensor products between sets. This notation is be understood for example as $\{1-\xi-\eta,\xi\} \otimes \{\mathbf{e}_1+\mathbf{e}_2,\mathbf{e}_1\} = \{(1-\xi-\eta)(\mathbf{e}_1+\mathbf{e}_2),(1-\xi-\eta)\mathbf{e}_1,\xi(\mathbf{e}_1+\mathbf{e}_2),\xi\mathbf{e}_1\}$.

2. Hilbert spaces and trace operators

Hilbert spaces are the natural function spaces in the formulation of variational problems [1]. In preparation for the construction of conforming subspaces we introduce the classical Hilbert spaces and their associated norms

$$H^1(V) = \{u \in L^2(V) \mid \nabla u \in [L^2(V)]^3\}\,, \qquad \|u\|^2_{H^1(V)} = \|u\|^2_{L^2} + \|\nabla u\|^2_{L^2}\,, \tag{2.1a}$$

$$H(\mathrm{curl}, V) = \{\mathbf{u} \in [L^2(V)]^3 \mid \mathrm{curl}\,\mathbf{u} \in [L^2(V)]^3\}\,, \qquad \|u\|^2_{H(\mathrm{curl},V)} = \|\mathbf{u}\|^2_{L^2} + \|\mathrm{curl}\,\mathbf{u}\|^2_{L^2}\,, \tag{2.1b}$$

$$H(\mathrm{div}, V) = \{\mathbf{u} \in [L^2(V)]^3 \mid \mathrm{div}\,\mathbf{u} \in L^2(V)\}\,, \qquad \|u\|^2_{H(\mathrm{div},V)} = \|\mathbf{u}\|^2_{L^2} + \|\mathrm{div}\,\mathbf{u}\|^2_{L^2}\,, \tag{2.1c}$$

which are based on the Lebesgue space

$$L^2(V) = \{u : V \to \mathbb{R} \mid \|u\|_{L^2(V)} < \infty\}\,, \qquad \|u\|^2_{L^2(V)} = \langle u, u\rangle_{L^2(V)} = \int_V u^2 \,\mathrm{d}V\,. \tag{2.2}$$

Note that on two-dimensional domains the differential operators are reduced to

$$\nabla u = \begin{bmatrix} u_{,x} \\ u_{,y} \end{bmatrix}\,, \qquad \mathrm{div}(\boldsymbol{R}\,\mathbf{u}) = u_{2,x} - u_{1,y}\,, \qquad \boldsymbol{R}\nabla u = \begin{bmatrix} u_{,y} \\ -u_{,x} \end{bmatrix}\,, \qquad \boldsymbol{R} = \begin{bmatrix} 0 & 1 \\ -1 & 0 \end{bmatrix}\,, \qquad \mathrm{div}\,\mathbf{u} = u_{1,x} + u_{2,y}\,, \tag{2.3}$$

such that two curl operators are introduced: one for two-dimensional vectors $\mathrm{div}(\boldsymbol{R}\,\cdot)$, and one for scalars $\boldsymbol{R}\nabla(\cdot)$. On contractible domains the Hilbert spaces are connected by the exact de Rham sequence [16–18,44], see Fig. 2.

Each Hilbert space is associated with a corresponding trace operator [45]. The trace of the function $u \in H^1(V)$ is defined by the bounded linear operator

$$\mathrm{tr}\,u = u\Big|_{\partial V} \in H^{1/2}(\partial V)\,, \qquad \exists\, c > 0 : \quad \|\mathrm{tr}\,u\|_{H^{1/2}(\partial V)} \le c\|u\|_{H^1(V)} \quad \forall\, u \in H^1(V)\,. \tag{2.4}$$

In other words, the trace restricts the function to the boundary of the domain. The trace of the $H(\mathrm{curl}, V)$ space is given by the tangential components on the boundary. On a surface the tangent vector is not unique, and therefore, the tangential projection is defined using the normal vector and the cross product

$$\mathrm{tr}^{\perp}_n\mathbf{u} = \mathbf{n} \times \mathbf{u}\Big|_{\partial V} \in [H^{-1/2}(\partial V)]^3\,, \qquad \exists\, c > 0 : \quad \|\mathrm{tr}^{\perp}_n\mathbf{u}\|_{H^{-1/2}(\partial V)} \le c\|\mathbf{u}\|_{H(\mathrm{curl},V)} \quad \forall\, \mathbf{u} \in H(\mathrm{curl}, V)\,. \tag{2.5}$$

For two-dimensional domains $A \subset \mathbb{R}^2$ the tangent vector is unique and the trace operator reduces to

$$\mathrm{tr}^{\parallel}_t\mathbf{u} = \langle \mathbf{t}, \mathbf{u}\rangle\Big|_{\partial A} \in H^{-1/2}(\partial A)\,. \tag{2.6}$$

Lastly, the trace of the $H(\mathrm{div}, V)$ space is defined by the normal projection at the boundary

$$\mathrm{tr}^{\parallel}_n\mathbf{u} = \langle \mathbf{n}, \mathbf{u}\rangle\Big|_{\partial V} \in H^{-1/2}(\partial V)\,, \qquad \exists\, c > 0 : \quad \|\mathrm{tr}^{\parallel}_n\mathbf{u}\|_{H^{-1/2}(\partial V)} \le c\|\mathbf{u}\|_{H(\mathrm{div},V)} \quad \forall\, \mathbf{u} \in H(\mathrm{div}, V)\,. \tag{2.7}$$

In this work we define the trace space via

$$H^{1/2}(\partial V) = \{v \in L^2(\partial V) \mid \exists\, u \in H^1(V) : \mathrm{tr}\,u = v\}\,, \tag{2.8}$$

and $H^{-1/2}(\partial V)$ is its dual. For a thorough treatment of fractional Sobolev spaces see [46], and [47] for the extended treatment of s-regularity on trace-spaces. The trace operators are used to define Hilbert spaces with boundary conditions. The exact de Rham sequence holds also on Hilbert spaces with vanishing traces, see Fig. 3. Further, the trace operators allow to identify finite elements of a specific Hilbert space via interface conditions. We state the interface theorem [23,48] and apply it to the construction of conforming subspaces.

Theorem 2.1 (*Interface Conditions*)**.** *A finite element space is a conforming subspace of a Hilbert space if and only if the jump of the trace of its elements vanishes for all arbitrarily defined interfaces $\Xi_{ij} = V_i \cap V_j\,, i \neq j$ where $V = V_i \cup V_j \subset \mathbb{R}^3$ and $\Xi_{ij} \subset \mathbb{R}^2$ (and analogously for two-dimensional domains)*

$$u \in H^1(V) \quad \Longleftrightarrow \quad [\![\mathrm{tr}\,u]\!]\Big|_{\Xi_{ij}} = 0 \quad \forall\, \Xi_{ij} = V_i \cap V_j\,, \tag{2.9a}$$

$$\mathbf{u} \in H(\mathrm{curl}, V) \quad \Longleftrightarrow \quad [\![\mathrm{tr}^{\perp}_n\mathbf{u}]\!]\Big|_{\Xi_{ij}} = 0 \quad \forall\, \Xi_{ij} = V_i \cap V_j\,, \tag{2.9b}$$

$$\mathbf{u} \in H(\mathrm{div}, V) \quad \Longleftrightarrow \quad [\![\mathrm{tr}^{\parallel}_n\mathbf{u}]\!]\Big|_{\Xi_{ij}} = 0 \quad \forall\, \Xi_{ij} = V_i \cap V_j\,. \tag{2.9c}$$

In the following sections the construction of arbitrary order $H(\mathrm{curl})$- and $H(\mathrm{div})$-conforming subspaces is presented. The construction is based on a polytopal association of base functions.

Definition 2.1 (*Polytopal Base Functions*)**.** Each base function is associated with its respective polytope and the underlying Hilbert space as follows:

$$\mathbb{R} \xrightarrow{\text{id}} H^1(V) \xrightarrow{\nabla} H(\text{curl}, V) \xrightarrow{\text{curl}} H(\text{div}, V) \xrightarrow{\text{div}} L^2(V)$$

$$\mathbb{R} \xrightarrow{\text{id}} H^1(A) \xrightarrow{\nabla} H(\text{curl}, A) \xrightarrow{\text{div}\boldsymbol{R}} L^2(A)$$

$$\mathbb{R} \xrightarrow{\text{id}} H^1(A) \xrightarrow{\boldsymbol{R}\nabla} H(\text{div}, A) \xrightarrow{\text{div}} L^2(A)$$

Fig. 2. Classical de Rham exact sequences for three- and two-dimensional contractible domains. The range of each operator is exactly the kernel of the next operator in the sequence.

$$\mathbb{R} \xrightarrow{\text{id}} H_0^1(V) \xrightarrow{\nabla} H_0(\text{curl}, V) \xrightarrow{\text{curl}} H_0(\text{div}, V) \xrightarrow{\text{div}} L_0^2(V)$$

$$\mathbb{R} \xrightarrow{\text{id}} H_0^1(A) \xrightarrow{\nabla} H_0(\text{curl}, A) \xrightarrow{\text{div}\boldsymbol{R}} L_0^2(A)$$

$$\mathbb{R} \xrightarrow{\text{id}} H_0^1(A) \xrightarrow{\boldsymbol{R}\nabla} H_0(\text{div}, A) \xrightarrow{\text{div}} L_0^2(A)$$

Fig. 3. De Rham exact sequences for Hilbert spaces with vanishing traces. The Lebesgue zero-space is characterized by functions with a vanishing integral over the domain.

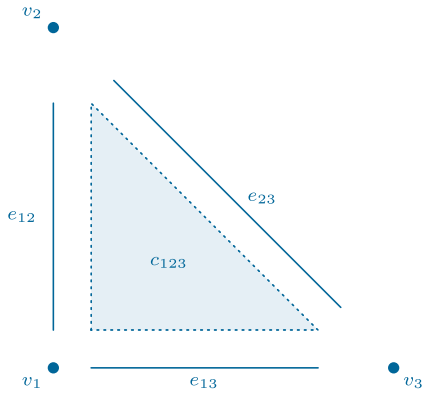

Fig. 4. Decomposition of the unit triangle into vertices, edges and the cell.

1. A vertex base function has a vanishing trace on all other vertices and non-neighbouring edges and faces.
2. An edge base function has a vanishing trace on all other edges and non-neighbouring faces.
3. A face base function has a vanishing trace on all other faces.
4. A cell base function has a vanishing trace on the entire boundary of the element.

The definition is general and the respective trace may change according to the corresponding Hilbert space.

3. Two-dimensional templates

This section is dedicated to the introduction of polytopal templates on the reference triangle

$$\Gamma = \{(\xi, \eta) \in [0, 1]^2 \mid \xi + \eta \leq 1\}\,. \tag{3.1}$$

To that end, the triangle is decomposed into its base polytopes given by its vertices $\{v_1, v_2, v_3\}$, its edges $\{e_{12}, e_{13}, e_{23}\}$, and its interior cell c_{123}, see Fig. 4. Further, each polytope is associated with base functions belonging to an H^1-conforming subspace $U^p(\Gamma)$ with $\dim U^p(\Gamma) = \dim P^p(\Gamma) = (p+2)(p+1)/2$.

Definition 3.1 (*Triangle $U^p(\Gamma)$-polytopal Spaces*)**.** Each polytope is associated with a space of base functions as follows:

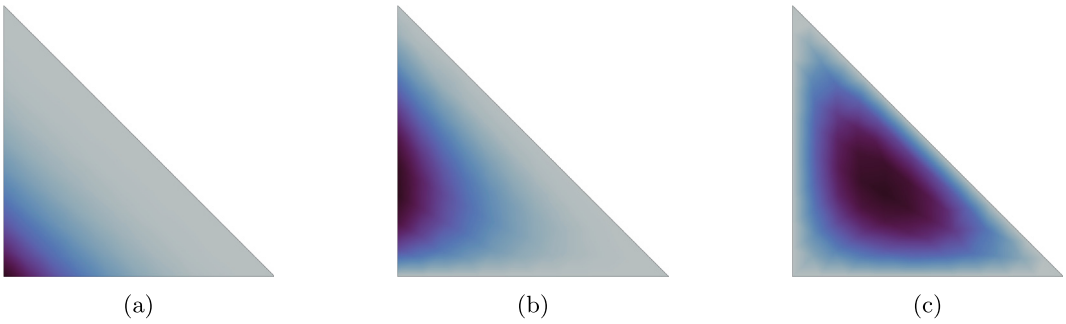

Fig. 5. Vertex (a), edge (b) and cell (c) base functions on the reference triangle. The transition from light to dark represents the increase in value of the function. The lowest value of each base function is zero and the maximum value may change according to the basis.

- Each vertex is associated with the space of its respective base function $\mathcal{V}_i^p(\Gamma)$. As such, there are three spaces in total $i \in \{1,2,3\}$ and each one is of dimension one, $\dim \mathcal{V}_i^p(\Gamma) = 1 \quad \forall\, i \in \{1,2,3\}$. The index p represents the polynomial order of the space, which is always 1 only for a hierarchical polynomial basis.
- For each edge there exists a space of edge functions $\mathcal{E}_j^p(\Gamma)$ with the multi-index $j \in \mathcal{J} = \{(1,2),(1,3),(2,3)\}$. The dimension of each edge space is given by $\dim \mathcal{E}_j^p(\Gamma) = p-1$.
- Lastly, the cell is equipped with the space of cell base functions $\mathcal{C}_{123}^p(\Gamma)$ with $\dim \mathcal{C}_{123}^p(\Gamma) = (p-2)(p-1)/2$.

The association with a respective polytope reflects Definition 2.1 with the trace operator for H^1-spaces.

A depiction of vertex, edge, and cell base functions is given in Fig. 5. Clearly, this is the standard definition of base functions for approximations in H^1. Common examples of such bases are Lagrange, Legendre [34,35] and Bernstein [40], or other hierarchical types [41].

In the following we define templates on the reference triangle, such that their multiplications with corresponding base functions from $U^p(\Gamma)$ generate vectorial base functions for either $H(\mathrm{curl})$ or $H(\mathrm{div})$. The Nédélec element of the second type and the Brezzi–Douglas–Marini element are defined to span complete polynomial spaces, $\operatorname{span} \mathcal{N}_{II}^p(\Gamma) = \operatorname{span} \mathcal{BDM}^p(\Gamma) = \operatorname{span}[P^p(\Gamma)]^2$. Consequently, at each polytope the corresponding template set $\mathcal{T}_i$ consists of two linearly independent vectors that span the Euclidean space, $\operatorname{span} \mathcal{T}_i = \operatorname{span} \mathbb{R}^2$. This is not the case for the Nédélec element of the first type and Raviart–Thomas elements, which are built using enriched polynomial spaces, $\dim \mathcal{N}_I^p(\Gamma) = \dim \mathcal{RT}^p(\Gamma) > \dim[P^p(\Gamma)]^2$. In latter cases, the template sets are used to complete the non-kernel base functions and their dimension is reduced.

3.1. Nédélec II

In order to construct a template for the Nédélec element of the second type [25] we consider the decomposition of the reference triangle in Fig. 4. On the first vertex v_1 we define a template vertex-edge vector $\boldsymbol{\ell}$ with a tangential projection of one on the unit tangent vector of the first edge e_{12} and a zero projection on the second edge e_{13}

$$\langle \mathbf{e}_2, \boldsymbol{\ell} \rangle = 1\,, \qquad \langle \mathbf{e}_1, \boldsymbol{\ell} \rangle = 0\,, \tag{3.2}$$

as depicted on the left triangle in Fig. 6. Next we define a vector with a projection of one on the tangent vector of the first edge e_{12}, choosing $\mathbf{e}_2$. Further, we construct a normal vector $-\mathbf{e}_1$ on the first edge e_{12}. Lastly, we define two unit vectors in the cell, $\mathbf{e}_1$ and $\mathbf{e}_2$. The remaining template vectors for their respective polytopes are computed by mapping the triangle c_{123} to various permutations of c_{ijk} on the unit domain via covariant Piola transformations (see Appendix A) and adjusting the sign to ensure a positive projection on the tangent vector as defined on the original reference triangle, such that it is always oriented from the lower indexed vertex to the higher indexed vertex (v_i and v_j s.t. $i < j$, solving the orientation problem, see Appendix B). The procedure is exemplified for the vertex-edge template vectors in Fig. 6, using the mappings

$$\boldsymbol{J} = \begin{bmatrix} \mathbf{x}_3 - \mathbf{x}_1 & \mathbf{x}_3 - \mathbf{x}_2 \end{bmatrix}, \qquad \boldsymbol{J}_{132} = \begin{bmatrix} 0 & 1 \\ 1 & 0 \end{bmatrix}, \qquad \boldsymbol{J}_{312} = \begin{bmatrix} 0 & 1 \\ -1 & -1 \end{bmatrix},$$
$$\boldsymbol{\ell} = \mathbf{e}_2\,, \qquad \boldsymbol{J}_{132}^{-T}\boldsymbol{\ell} = \mathbf{e}_1\,, \qquad \boldsymbol{J}_{312}^{-T}\boldsymbol{\ell} = \mathbf{e}_1\,, \tag{3.3}$$

which result from the vertex permutations and the corresponding affine mappings in the depiction via the Jacobi matrix $\boldsymbol{J}$. We note that in general, Piola transformations change the size of vectors, such that the resulting template vectors are not necessarily unitary. However, the size of their tangential projection with respect to the non-unitary tangent vector of an edge is maintained by the transformation, asserting consistency (compare with Appendix B). The complete template is depicted in Fig. 7.

Remark 3.1. The polytopal set is not unique and depends on the initial definition on the first polytopes of choice and the resulting mapping. Further, one can change pure edge-type template vectors by adding or subtracting normal vectors without influencing the

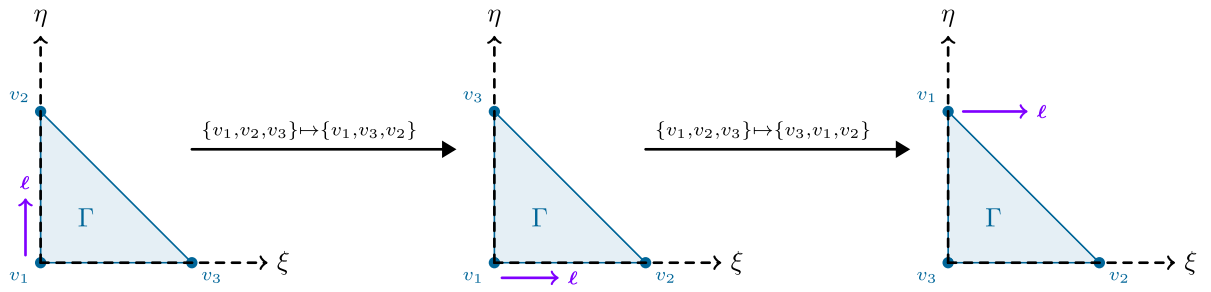

Fig. 6. Derivation of template vectors from the first definition for the remaining edges via permutations of the reference triangle using covariant Piola mappings. The depiction exemplifies how the first vertex-edge template vector ℓ corresponding to the vertex v_1 and edge e_{12}, is used to derive the vertex-edge template vectors of v_1–e_{13} and v_2–e_{23}.

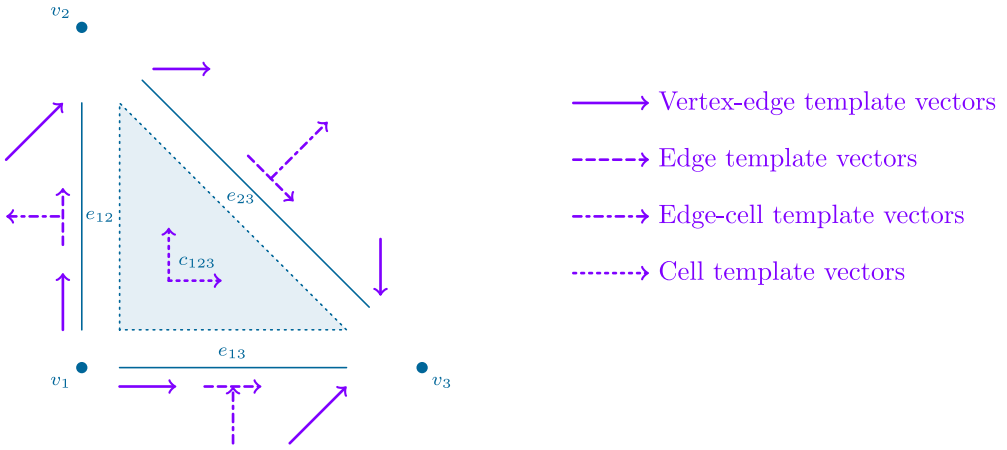

Fig. 7. Template vectors for the reference Nédélec triangle element of the second type on their corresponding polytope. Each vertex is endowed with two template vectors, one for each of its intersecting edges. Each edge is equipped with two template vectors, one for its tangent and one normal edge-cell vector for the cell. Finally, the cell is endowed with the Cartesian basis.

tangential projection. This does not influence the tangential regularity of the element, since the normal component on an edge is endowed with its own edge-cell-type degree of freedom and can thus jump between interfacing elements.

The resulting template is given by the super-set of the sets for the respective polytopes

$$\mathcal{T} = \{\mathcal{T}_1, \mathcal{T}_2, \mathcal{T}_3, \mathcal{T}_{12}, \mathcal{T}_{13}, \mathcal{T}_{23}, \mathcal{T}_{123}\}, \tag{3.4}$$

where the polytopal sets read

$$\begin{aligned} &\mathcal{T}_1 = \{\mathbf{e}_1, \mathbf{e}_2\}, && \mathcal{T}_2 = \{\mathbf{e}_1 + \mathbf{e}_2, \mathbf{e}_1\}, && \mathcal{T}_3 = \{\mathbf{e}_1 + \mathbf{e}_2, -\mathbf{e}_2\}, \\ &\mathcal{T}_{12} = \{\mathbf{e}_2, -\mathbf{e}_1\}, && \mathcal{T}_{13} = \{\mathbf{e}_1, \mathbf{e}_2\}, && \mathcal{T}_{23} = \{(1/2)(\mathbf{e}_1 - \mathbf{e}_2), \mathbf{e}_1 + \mathbf{e}_2\}, \\ &\mathcal{T}_{123} = \{\mathbf{e}_1, \mathbf{e}_2\}. \end{aligned} \tag{3.5}$$

The set can now be used in conjunction with an underlying $U^p(\Gamma)$-space to construct a Nédélec element of the second type of order p on the reference domain

$$\mathcal{N}^p_{II}(\Gamma) = \left\{ \bigoplus_{i=1}^{3} \mathcal{V}^p_i(\Gamma) \otimes \mathcal{T}_i \right\} \oplus \left\{ \bigoplus_{j\in\mathcal{J}} \mathcal{E}^p_j(\Gamma) \otimes \mathcal{T}_j \right\} \oplus \{C^p_{123}(\Gamma) \otimes \mathcal{T}_{123}\}, \qquad \mathcal{J} = \{(1,2),(1,3),(2,3)\}, \tag{3.6}$$

where $\mathcal{V}^p_i(\Gamma)$ are the sets of the vertex base functions, $\mathcal{E}^p_j(\Gamma)$ are the sets of edge base functions and $C^p_{123}(\Gamma)$ is the set of cell base functions.

Definition 3.2 (*Triangle $\mathcal{N}^p_{II}$ Base Functions*)**.** The base functions of the triangle Nédélec element of the second type are defined on their respective polytope as follows.

- On each edge e_{ij} with vertices v_i and v_j, the base functions read

$$\text{Vertex-edge:} \quad \vartheta(\xi,\eta) = n\mathscr{t}\,, \quad n \in \mathcal{V}_i^p\,, \quad \mathscr{t} \in \left\{ \mathscr{t} \in \mathcal{T}_i \mid \mathrm{tr}_t^{\parallel}\mathscr{t}\Big|_{e_{ij}} \neq 0 \right\}, \tag{3.7a}$$

$$\vartheta(\xi,\eta) = n\mathscr{t}\,, \quad n \in \mathcal{V}_j^p\,, \quad \mathscr{t} \in \left\{ \mathscr{t} \in \mathcal{T}_j \mid \mathrm{tr}_t^{\parallel}\mathscr{t}\Big|_{e_{ij}} \neq 0 \right\}, \tag{3.7b}$$

$$\text{Edge:} \quad \vartheta(\xi,\eta) = n\mathscr{t}\,, \quad n \in \mathcal{E}_{ij}^p\,, \quad \mathscr{t} \in \left\{ \mathscr{t} \in \mathcal{T}_{ij} \mid \mathrm{tr}_t^{\parallel}\mathscr{t}\Big|_{e_{ij}} \neq 0 \right\}, \tag{3.7c}$$

  such that $\mathscr{t}$ is an element of the template sets, whose tangential trace does not vanish on the edge.
- The cell base functions are given by

$$\text{Edge-cell:} \quad \vartheta(\xi,\eta) = n\mathscr{t}\,, \quad n \in \mathcal{E}_{12}^p\,, \quad \mathscr{t} \in \left\{ \mathscr{t} \in \mathcal{T}_{12} \mid \mathrm{tr}_t^{\parallel}\mathscr{t}\Big|_{e_{12}} = 0 \right\}, \tag{3.8a}$$

$$\vartheta(\xi,\eta) = n\mathscr{t}\,, \quad n \in \mathcal{E}_{13}^p\,, \quad \mathscr{t} \in \left\{ \mathscr{t} \in \mathcal{T}_{13} \mid \mathrm{tr}_t^{\parallel}\mathscr{t}\Big|_{e_{13}} = 0 \right\}, \tag{3.8b}$$

$$\vartheta(\xi,\eta) = n\mathscr{t}\,, \quad n \in \mathcal{E}_{23}^p\,, \quad \mathscr{t} \in \left\{ \mathscr{t} \in \mathcal{T}_{23} \mid \mathrm{tr}_t^{\parallel}\mathscr{t}\Big|_{e_{23}} = 0 \right\}, \tag{3.8c}$$

$$\text{Cell:} \quad \vartheta(\xi,\eta) = n\mathscr{t}\,, \quad n \in \mathcal{C}_{123}^p\,, \quad \mathscr{t} \in \mathcal{T}_{123}\,, \tag{3.8d}$$

  such that their tangential trace vanishes on all edges.

A selection of cubic $\mathcal{N}_{II}^p(\Gamma)$-base functions given by the construction is depicted in Fig. 8.

Theorem 3.1 (*Linear Independence*). *The tensor product of the template with an $H^1(\Gamma)$-conforming polynomial basis $U^p(\Gamma) \subset H^1(\Gamma)$ yields a linearly independent basis for the Nédélec element of the second type.*

Proof. Under the assertion that the underlying $H^1(\Gamma)$-conforming polynomial basis $U^p(\Gamma) \subset H^1(\Gamma)$ is linearly independent, linear independence of the $\mathcal{N}_{II}^p(\Gamma)$ basis follows automatically since each base function $n \in U^p$ is multiplied with two linearly independent vectors $\mathscr{t} \in \mathcal{T}_i$, thus inheriting the linear independence of the basis on the vectorial level due to $\mathrm{span}\,\mathcal{T}_i = \mathrm{span}\,\mathbb{R}^2$. Further, the resulting basis has the required dimensionality

$$\dim[U^p(\Gamma)]^2 = \dim[P^p(\Gamma)]^2 = \dim \mathcal{N}_{II}^p(\Gamma)\,, \tag{3.9}$$

of the Nédélec finite element space. □

Theorem 3.2 ($H(\mathrm{curl}, A)$-*conformity*). *The constructed element on the reference domain Γ is $H(\mathrm{curl}, A)$-conforming under covariant Piola transformations of the base functions.*

Proof. By construction, the tangential projection of each non-cell base function on the tangential vector of its respective polytope is the underlying H^1-conforming base function

$$\langle \boldsymbol{\tau},\, \vartheta_i \rangle = n_i\,. \tag{3.10}$$

Since the templates are constructed by permutations of the reference element, this characteristic is extended to every corresponding polytope. Lastly, the covariant Piola transformations uphold the tangential projections in the physical domain [1,34] (compare with Appendix A). As such, the condition at the interfaces of neighbouring elements A_i and A_j is $[\![\mathrm{tr}_t^{\parallel}\mathbf{u}]\!]|_{\Xi_{ij}} = [\![\mathrm{tr}\,\langle \mathbf{t},\, \mathbf{u}\rangle]\!]|_{\Xi_{ij}} = c_{ij}(n_i - n_j) = 0$ for the tangential components. This property is upheld by the underlying $H^1(A)$-conforming subspace, since the constant c_{ij} and the base functions n_i and n_j are the same for the interfacing elements A_i and A_j. □

3.2. Brezzi-Douglas-Marini

Next we construct the template for the Brezzi–Douglas–Marini element [26] on the reference triangle. The procedure is analogous to the one for the Nédélec element. We define two normal vectors for the vertex v_1 with respect to its intersecting edges, one normal vector and one tangent vector on e_{12} and the Cartesian basis in the cell c_{123}. By permutations of the reference triangle c_{ijk} via contravariant Piola transformations (see Appendix A) we retrieve the remaining template vectors, compare with Fig. 6. The sign of the vectors is adjusted in order to ensure conformal normal projections on the edge normals. Further, on the slanted edge, we modify the edge normal with the tangential vector to generate an orthogonal template. The resulting template is depicted in Fig. 9 and is given by the super-set of the sets belonging to the respective polytopes

$$\mathcal{T} = \{\mathcal{T}_1, \mathcal{T}_2, \mathcal{T}_3, \mathcal{T}_{12}, \mathcal{T}_{13}, \mathcal{T}_{23}, \mathcal{T}_{123}\}\,, \tag{3.11}$$

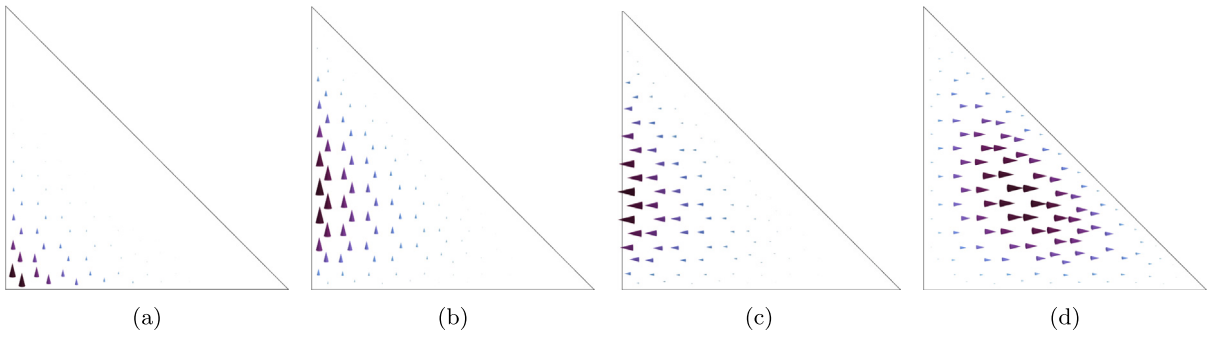

Fig. 8. Cubic vertex-edge (a), edge (b), edge-cell (c) and pure cell (d) vectorial base functions of the Nédélec element of the second type on the reference triangle. The colour and size of the arrows represents the intensity of the field.

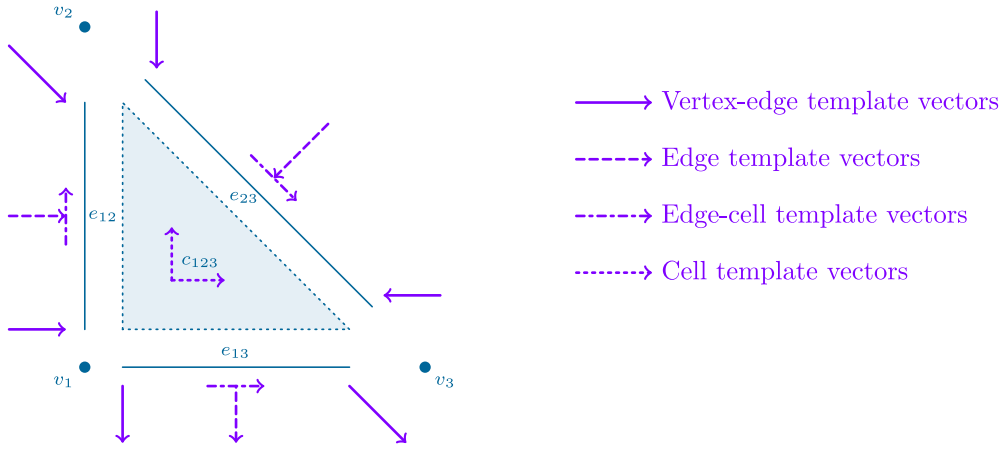

Fig. 9. Template vectors for the reference Brezzi–Douglas–Marini triangle element on their corresponding polytope. Each vertex is endowed with two template vectors, one for each of its intersecting edges and their respective normals. Each edge is equipped with two template vectors, one for its normal and one tangent edge-cell vector for the cell. Finally, the cell is endowed with the Cartesian basis.

where the polytopal sets read

$$\begin{aligned}
&\mathcal{T}_1 = \{\mathbf{e}_1, -\mathbf{e}_2\}, && \mathcal{T}_2 = \{\mathbf{e}_1 - \mathbf{e}_2, -\mathbf{e}_2\}, && \mathcal{T}_3 = \{\mathbf{e}_1 - \mathbf{e}_2, -\mathbf{e}_1\}, \\
&\mathcal{T}_{12} = \{\mathbf{e}_1, \mathbf{e}_2\}, && \mathcal{T}_{13} = \{-\mathbf{e}_2, \mathbf{e}_1\}, && \mathcal{T}_{23} = \{-(1/2)(\mathbf{e}_1 + \mathbf{e}_2), \mathbf{e}_2 - \mathbf{e}_1\}, \\
&\mathcal{T}_{123} = \{\mathbf{e}_1, \mathbf{e}_2\}. && && \qquad (3.12)
\end{aligned}$$

With the polytopal template at hand, we can construct the Brezzi–Douglas–Marini element by tensor products with an underlying $U^p(\Gamma)$-basis

$$\mathcal{BDM}^p(\Gamma) = \left\{ \bigoplus_{i=1}^{3} \mathcal{V}_i^p(\Gamma) \otimes \mathcal{T}_i \right\} \oplus \left\{ \bigoplus_{j \in \mathcal{J}} \mathcal{E}_j^p(\Gamma) \otimes \mathcal{T}_j \right\} \oplus \{ C_{123}^p(\Gamma) \otimes \mathcal{T}_{123} \}, \qquad \mathcal{J} = \{(1,2),(1,3),(2,3)\}, \qquad (3.13)$$

where $\mathcal{V}_i^p(\Gamma)$ are the sets of vertex base functions, $\mathcal{E}_j^p(\Gamma)$ contain the edge base functions and $C_{123}^p(\Gamma)$ is the set of cell base functions.

Definition 3.3 (*Triangle $\mathcal{BDM}^p$ Base Functions*)**.** The base functions of the triangle Brezzi–Douglas–Marini element are defined on their respective polytopes as follows.

- On each edge e_{ij} with vertices v_i and v_j, the base functions read

$$\text{Vertex-edge:} \qquad \boldsymbol{\phi}(\xi,\eta) = n\boldsymbol{\ell}, \qquad n \in \mathcal{V}_i^p, \qquad \boldsymbol{\ell} \in \left\{ \boldsymbol{\ell} \in \mathcal{T}_i \mid \mathrm{tr}_n^{\parallel} \boldsymbol{\ell} \Big|_{e_{ij}} \neq 0 \right\}, \qquad (3.14a)$$

$$\boldsymbol{\phi}(\xi,\eta) = n\boldsymbol{\ell}, \qquad n \in \mathcal{V}_j^p, \qquad \boldsymbol{\ell} \in \left\{ \boldsymbol{\ell} \in \mathcal{T}_j \mid \mathrm{tr}_n^{\parallel} \boldsymbol{\ell} \Big|_{e_{ij}} \neq 0 \right\}, \qquad (3.14b)$$

$$\text{Edge:} \qquad \boldsymbol{\phi}(\xi,\eta) = n\mathscr{C}\,, \qquad n \in \mathcal{E}^p_{ij}\,, \qquad \mathscr{C} \in \left\{ \mathscr{C} \in \mathcal{T}_{ij} \mid \mathrm{tr}^{\parallel}_n \mathscr{C}\Big|_{e_{ij}} \neq 0 \right\}, \tag{3.14c}$$

such that $\mathscr{C}$ is an element of the template sets, whose normal trace does not vanish on the edge.

- The cell base functions are given by all permutations of

$$\text{Edge-cell:} \qquad \boldsymbol{\phi}(\xi,\eta) = n\mathscr{C}\,, \qquad n \in \mathcal{E}^p_{12}\,, \qquad \mathscr{C} \in \left\{ \mathscr{C} \in \mathcal{T}_{12} \mid \mathrm{tr}^{\parallel}_n \mathscr{C}\Big|_{e_{12}} = 0 \right\}, \tag{3.15a}$$

$$\boldsymbol{\phi}(\xi,\eta) = n\mathscr{C}\,, \qquad n \in \mathcal{E}^p_{13}\,, \qquad \mathscr{C} \in \left\{ \mathscr{C} \in \mathcal{T}_{13} \mid \mathrm{tr}^{\parallel}_n \mathscr{C}\Big|_{e_{13}} = 0 \right\}, \tag{3.15b}$$

$$\boldsymbol{\phi}(\xi,\eta) = n\mathscr{C}\,, \qquad n \in \mathcal{E}^p_{23}\,, \qquad \mathscr{C} \in \left\{ \mathscr{C} \in \mathcal{T}_{23} \mid \mathrm{tr}^{\parallel}_n \mathscr{C}\Big|_{e_{23}} = 0 \right\}, \tag{3.15c}$$

$$\text{Cell:} \qquad \boldsymbol{\phi}(\xi,\eta) = n\mathscr{C}\,, \qquad n \in C^p_{123}\,, \qquad \mathscr{C} \in \mathcal{T}_{123}\,, \tag{3.15d}$$

such that their normal trace vanishes on all edges.

A depiction of cubic base functions is given in Fig. 10.

Theorem 3.3 (*Linear Independence*)**.** *The tensor product of the template with an $H^1(\Gamma)$-conforming polynomial basis $U^p(\Gamma) \subset H^1(\Gamma)$ yields a linearly independent basis for the Brezzi–Douglas–Marini element.*

Proof. The proof is analogous to the one for the $\mathcal{N}^p_{II}$-space Theorem 3.1, since the Brezzi–Douglas–Marini element can be constructed by rotating the base functions of a Nédélec element of the second type by 90 degrees. □

Theorem 3.4 ($H(\mathrm{div}, A)$*-conformity*)**.** *The constructed element on the reference domain Γ is $H(\mathrm{div}, A)$-conforming under contravariant Piola transformations of the base functions.*

Proof. By design, the non-cell base functions exhibit the property

$$\langle \boldsymbol{\nu}, \boldsymbol{\phi}_i \rangle = n_i\,, \tag{3.16}$$

on their corresponding edges due to their construction by permutations of the reference triangle with contravariant Piola transformations. The property is maintained by contravariant Piola transformation to the physical domain [1,34] (see Appendix A). Consequently, the interface condition between neighbouring elements $[\![\mathrm{tr}^{\parallel}_n \mathbf{u}]\!]|_{\Xi_{ij}} = 0$ is given by $[\![\mathrm{tr}\,\langle \mathbf{n}, \mathbf{u}\rangle]\!]|_{\Xi_{ij}} = c_{ij}(n_i - n_j) = 0$ for the normal components, which is satisfied by the underlying subspace $U^p(A)$. □

3.3. Nédélec I

The Nédélec element of the second type has the disadvantage that its curl is a polynomial space of a lower degree $\mathrm{div}(\boldsymbol{R}\,\mathcal{N}^p_{II}) = P^{p-1}$. Consequently, one loses one order of convergence in the curl terms. In order to ameliorate the convergence rate one can employ the Nédélec elements of the first type [24], which enhance the polynomial space with base functions not in the kernel of the curl operator $\boldsymbol{\vartheta}_i \notin \ker(\mathrm{div}\boldsymbol{R})$

$$\dim \mathcal{N}^p_I(\Gamma) = \dim([P^p(\Gamma)]^2 \oplus \boldsymbol{R}\widetilde{P}^p(\Gamma)\boldsymbol{\xi}) = (p+3)(p+1)\,, \qquad p \geq 0\,, \tag{3.17}$$

such that $\mathcal{N}^p_{II} \subset \mathcal{N}^p_I$. The polynomial space $[P^p(\Gamma)]^2 \oplus \boldsymbol{R}\widetilde{P}^p(\Gamma)\boldsymbol{\xi}$ is used to construct the Nédélec base functions on the reference triangle, where $\widetilde{P}^p(\Gamma)$ is the space of homogeneous polynomials of order p on Γ. In order to enhance the space, one must be able to split the space between kernel functions and non-kernel functions while maintaining conformity. Here we follow the ideas presented in [34,35], where one explicitly applies the operators in the exact polynomial sequences to construct the kernel of the next space. We complement the kernel space with our new approach and introduce a specific and intuitive polytopal template leading to non-kernel base functions.

We start with the kernel of $\mathcal{N}^p_I(\Gamma)$ by taking gradients of the base functions of the $U^{p+1}(\Gamma)$ space while excluding the vertex base functions

$$\boldsymbol{\vartheta}_i(\xi,\eta) = \nabla_\xi n_i^{p+1}\,. \tag{3.18}$$

This yields $(p+2)(p+1)/2 - 3$ base functions. We augment the space by adding the lowest order $\mathcal{N}^0_I(\Gamma)$ base functions [29], see Fig. 11,

$$\boldsymbol{\vartheta}^I_1(\xi,\eta) = \begin{bmatrix} \eta \\ 1-\xi \end{bmatrix}, \qquad \boldsymbol{\vartheta}^I_2(\xi,\eta) = \begin{bmatrix} 1-\eta \\ \xi \end{bmatrix}, \qquad \boldsymbol{\vartheta}^I_3(\xi,\eta) = \begin{bmatrix} \eta \\ -\xi \end{bmatrix}. \tag{3.19}$$

Next we need to enhance the space with a minimal number of base functions belonging to a higher degree polynomial space such that $\dim[\mathrm{div}(\boldsymbol{R}\,\mathcal{N}^p_I(\Gamma))] = \dim P^p(\Gamma) = (p+2)(p+1)/2$ base functions are found and the curl spans the next polynomial space in the sequence. In order to do so we introduce the polytopal template

$$\mathcal{T} = \{\mathcal{T}_1, \mathcal{T}_2, \mathcal{T}_{12}, \mathcal{T}_{13}, \mathcal{T}_{23}, \mathcal{T}_{123}\}\,, \tag{3.20}$$

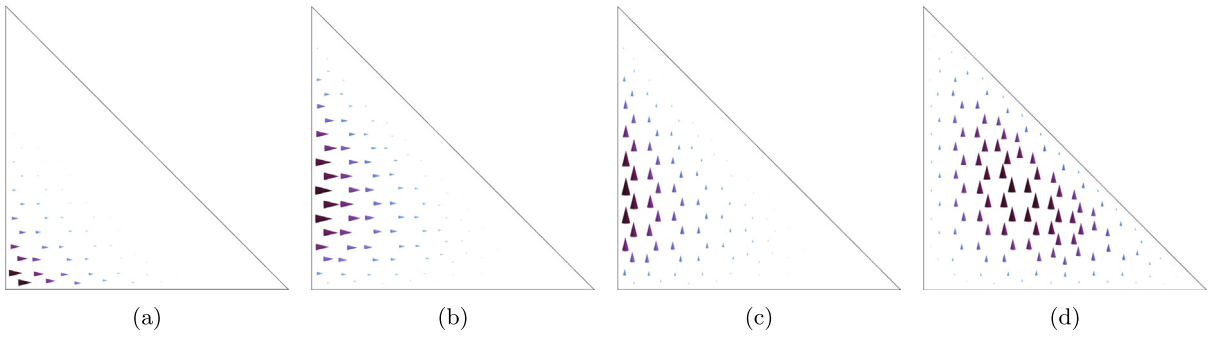

Fig. 10. Cubic vertex-edge (a), edge (b), edge-cell (c) and pure cell (d) base functions of the Brezzi–Douglas–Marini element on the reference triangle.

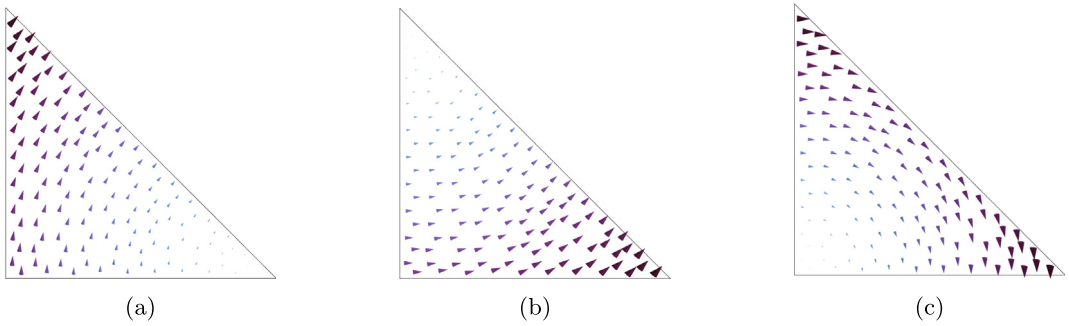

Fig. 11. The base functions of the lowest order Nédélec element of the first type on the reference triangle belonging to the first (a), second (b) and third (c) edges.

where the polytopal sets are derived from the lowest order Nédélec base functions of the first type (Eq. (3.19))

$$\begin{aligned} &\mathcal{T}_1 = \{\boldsymbol{\vartheta}_3^I\}, && \mathcal{T}_2 = \{\boldsymbol{\vartheta}_2^I\}, && \mathcal{T}_{12} = \{\boldsymbol{\vartheta}_3^I - \boldsymbol{\vartheta}_2^I\}, \\ &\mathcal{T}_{13} = \{\boldsymbol{\vartheta}_1^I + \boldsymbol{\vartheta}_3^I\}, && \mathcal{T}_{23} = \{\boldsymbol{\vartheta}_1^I - \boldsymbol{\vartheta}_2^I\}, && \mathcal{T}_{123} = \{\boldsymbol{\vartheta}_1^I - \boldsymbol{\vartheta}_2^I + \boldsymbol{\vartheta}_3^I\}. \end{aligned} \tag{3.21}$$

From the depiction in Fig. 12 it is intuitively apparent that the template vectors represent the components needed to generate rotational flux. In fact, the template is composed of shifted and scaled linear vortex fields, centred around their respective polytopes. The non-gradient base functions are given by the tensor product

$$\left\{\bigoplus_{i=1}^{2} \mathcal{V}_i^p(\Gamma) \otimes \mathcal{T}_i\right\} \oplus \left\{\bigoplus_{j\in\mathcal{J}} \mathcal{E}_j^p(\Gamma) \otimes \mathcal{T}_j\right\} \oplus \{\mathcal{C}_{123}^p(\Gamma) \otimes \mathcal{T}_{123}\}, \qquad \mathcal{J} = \{(1,2),(1,3),(2,3)\}. \tag{3.22}$$

This generates exactly $2p + (p-1)p/2$ base functions. Adding the constants from $\dim[\mathrm{div}(\boldsymbol{R}\,\mathcal{N}_I^0(\Gamma))] = 1$ satisfies the dimensionality of the next polynomial space in the sequence $2p + (p-1)p/2 + 1 = (p+2)(p+1)/2 = \dim P^p(\Gamma)$. Further, since $\boldsymbol{\vartheta}_i^I$ belong to $[P^0(\Gamma)]^2 \oplus \boldsymbol{R}\widetilde{P}^0(\Gamma)\boldsymbol{\xi}$ the resulting base functions $n_i^p \boldsymbol{\vartheta}_j^I$ clearly belong to $[P^p(\Gamma)]^2 \oplus \boldsymbol{R}\widetilde{P}^p(\Gamma)\boldsymbol{\xi}$. The complete Nédélec space reads

$$\begin{aligned} &\mathcal{N}_I^p(\Gamma) = \mathcal{N}_I^0(\Gamma) \oplus \left\{\bigoplus_{j\in\mathcal{J}} \nabla\mathcal{E}_j^{p+1}(\Gamma)\right\} \oplus \nabla\mathcal{C}_{123}^{p+1}(\Gamma) \oplus \left\{\bigoplus_{i=1}^{2} \mathcal{V}_i^p(\Gamma) \otimes \mathcal{T}_i\right\} \oplus \left\{\bigoplus_{j\in\mathcal{J}} \mathcal{E}_j^p(\Gamma) \otimes \mathcal{T}_j\right\} \oplus \{\mathcal{C}_{123}^p(\Gamma) \otimes \mathcal{T}_{123}\}, \\ &\mathcal{J} = \{(1,2),(1,3),(2,3)\}. \end{aligned} \tag{3.23}$$

Using the template and the exact sequence we can state the base functions for the Nédélec element of the first type.

Definition 3.4 (*Triangle $\mathcal{N}_I^p$ Base Functions*)**.** The base functions of the triangle Nédélec element of the first type are defined on their respective polytope as follows.

- On each edge e_{ij} the base functions read

$$\text{Edge:} \qquad \boldsymbol{\vartheta}(\xi,\eta) = \boldsymbol{\vartheta}^I, \qquad \boldsymbol{\vartheta}^I \in \left\{\boldsymbol{\vartheta} \in \mathcal{N}_I^0 \mid \mathrm{tr}_t^{\parallel}\boldsymbol{\vartheta}\Big|_{e_{ij}} \neq 0\right\}, \tag{3.24a}$$

$$\boldsymbol{\vartheta}(\xi,\eta) = \nabla_{\xi} n, \qquad n \in \mathcal{E}_{ij}^{p+1}, \tag{3.24b}$$

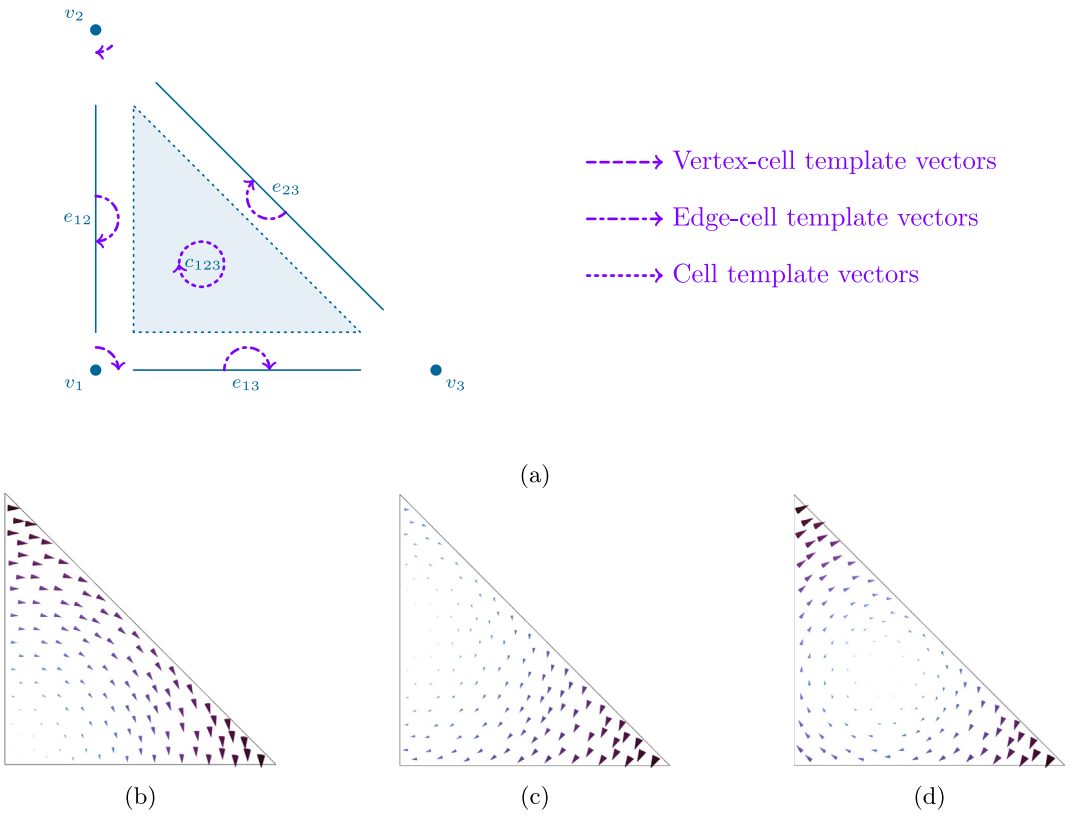

Fig. 12. Template vectors on the reference triangle for base functions orthogonal to the kernel of the curl operator (a). The template of the first vertex (b), followed by the template of the first edge (c) and lastly, the cell template (d).

- The cell base functions are given by

$$\text{Vertex-cell:} \quad \vartheta(\xi,\eta) = n\ell\,, \quad n \in \mathcal{V}_1^p\,, \quad \ell \in \mathcal{T}_1\,, \tag{3.25a}$$
$$\vartheta(\xi,\eta) = n\ell\,, \quad n \in \mathcal{V}_2^p\,, \quad \ell \in \mathcal{T}_2\,, \tag{3.25b}$$
$$\text{Edge-cell:} \quad \vartheta(\xi,\eta) = n\ell\,, \quad n \in \mathcal{E}_{12}^p\,, \quad \ell \in \mathcal{T}_{12}\,, \tag{3.25c}$$
$$\vartheta(\xi,\eta) = n\ell\,, \quad n \in \mathcal{E}_{13}^p\,, \quad \ell \in \mathcal{T}_{13}\,, \tag{3.25d}$$
$$\vartheta(\xi,\eta) = n\ell\,, \quad n \in \mathcal{E}_{23}^p\,, \quad \ell \in \mathcal{T}_{23}\,, \tag{3.25e}$$
$$\text{Cell:} \quad \vartheta(\xi,\eta) = n\ell\,, \quad n \in \mathcal{C}_{123}^p\,, \quad \ell \in \mathcal{T}_{123}\,, \tag{3.25f}$$
$$\vartheta(\xi,\eta) = \nabla_\xi n\,, \quad n \in \mathcal{C}_{123}^{p+1}\,, \tag{3.25g}$$

  such that their tangential trace vanishes on all edges. This holds true for the cell gradients due to the exactness of the de Rham sequence in Fig. 3.

A depiction of the higher order base functions is given in Fig. 13.

Theorem 3.5 (*Linear Independence*). *The set of base functions given by the lowest order Nédélec elements, the gradients of an $H^1(\Gamma)$-conforming polynomial subspace $U^{p+1}(\Gamma)$ (excluding vertex base functions) and the tensor product of the $U^p(\Gamma)$ base functions with the polytopal template yield a linearly independent polynomial basis for $\mathcal{N}_I^p(\Gamma)$.*

Proof. We start by showing the gradients of the $U^p(\Gamma)$ base functions are linearly independent of each other by using contradiction. Assume the set of gradients is linearly dependent, then there holds

$$\sum_i c_i \nabla_\xi n_i = \nabla_\xi \sum_i c_i n_i = 0\,, \tag{3.26}$$

for some combination of constants c_i where not all c_i values are zero. However, the vertex base functions are not employed. Thus, if the basis satisfies the partition of unity property, then the kernel of the gradient operator, namely constants $\mathbb{R}$, is missing and

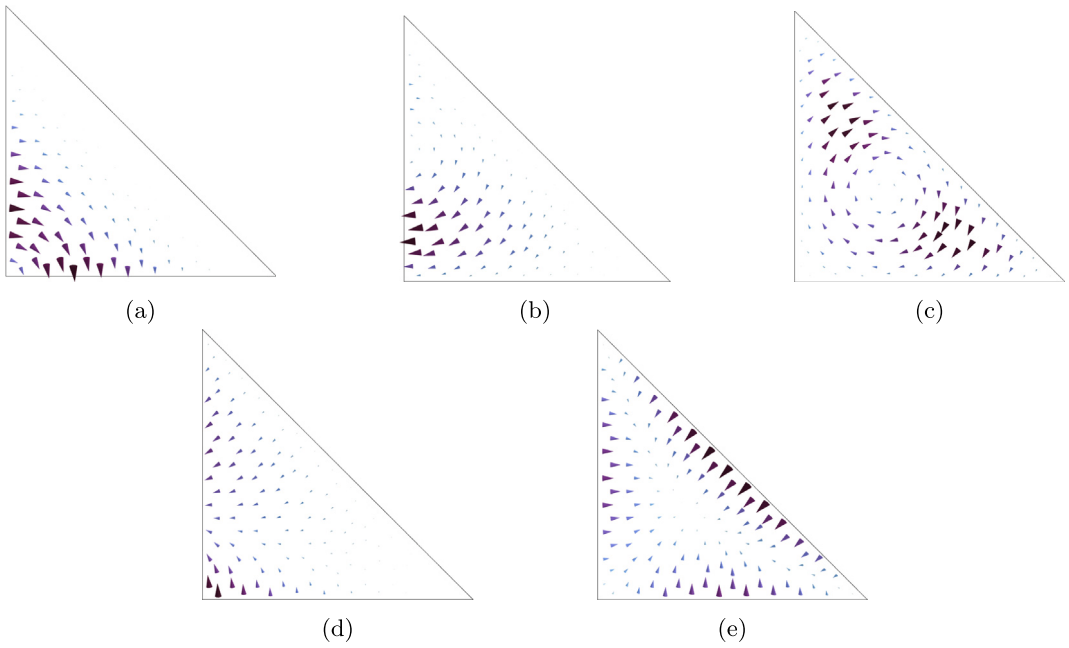

Fig. 13. Non-gradient vertex-cell (a), edge-cell (b) and pure cell (c) base functions. Gradient edge (d) and cell (e) base functions. The base functions belong to the Nédélec element of the first type and are depicted on the reference triangle.

the exact sequence property yields a contradiction (see Fig. 2). The same holds true for a hierarchical polynomial basis, since the vertex base functions are used to capture constants.

The base functions of the lowest order Nédélec elements of the first type are linearly independent of the gradients since their tangential traces on the edges of the triangle are constant $\mathrm{tr}_t^{\parallel} \boldsymbol{\vartheta}_i^I|_{\mu_i} \in \mathbb{R}$, whereas the tangential traces of the edge gradients are at least linear and the tangential traces of the cell gradients vanish on the entire boundary by the exact sequence property, compare Fig. 3. Together, the three lowest order base functions span the constant space $[P^0(\Gamma)]^2 = \mathbb{R}^2$. Further, their curls span the constant space $\mathbb{R}$.

In order to complete the proof we must show that the remaining base functions are non-gradients and linearly independent of the lowest order base functions. Observe that the template vectors have the general form

$$\boldsymbol{\vartheta}^I = \begin{bmatrix} c_1\eta - c_2 \\ c_3 - c_1\xi \end{bmatrix}, \qquad c_1 \in \{1,2,3\}, \qquad c_2, c_3 \in \{0,1\}, \tag{3.27}$$

such that the curl of the base function reads

$$\mathrm{div}_\xi(\boldsymbol{R} n \boldsymbol{\vartheta}^I) = \langle \nabla_\xi n,\ \boldsymbol{R}\boldsymbol{\vartheta}^I \rangle - 2c_1 n = (c_3 - c_1\xi) n_{,\xi} + (c_2 - c_1\eta) n_{,\eta} - 2c_1 n\,. \tag{3.28}$$

Clearly, the polynomial order of the underlying scalar base function n is maintained under the curl operator. Therefore, there holds

$$\mathrm{div}_\xi(\boldsymbol{R}[c_1 \boldsymbol{R}\boldsymbol{\xi} + \mathbf{c}] P^p(\Gamma)) = P^p(\Gamma), \qquad \mathbf{c} = \begin{bmatrix} -c_2 \\ c_3 \end{bmatrix}, \tag{3.29}$$

such that

$$\mathrm{div}_\xi(\boldsymbol{R} \sum_{i=0}^{p} c_i n_i \boldsymbol{\vartheta}^I) = 0 \quad \Longleftrightarrow \quad c_i = 0 \quad \forall\, i \in \{0,1,\dots,p\}, \tag{3.30}$$

by dimensionality. The latter is readily observed when a hierarchical polynomial basis is used. If the complete span of n_i functions is employed, then the constant element is present and the curl operator maps also to the space of constants $\mathbb{R}$. However, this space is already obtained by employing the $\mathcal{N}_I^0$-basis in the construction and as such, leads to linear dependence. By removing the last vertex base function, the hierarchical basis no longer contains the space of constants, thus asserting linear independence of the total construction. The same holds true for any other basis that satisfies the partition of unity property since removing one base function cancels this characteristic and removes the constant element from the space. □

Theorem 3.6 ($H(\mathrm{curl}, A)$*-conformity*)**.** *The resulting finite element is* $H(\mathrm{curl}, A)$*-conforming under covariant Piola mappings.*

Proof. The lowest order Nédélec base functions are $H(\mathrm{curl}, A)$-conforming by their degrees of freedom [24]. The gradient base functions are conforming due to the exact sequence property $\nabla H^1(A) \subset H(\mathrm{curl}, A)$, see Fig. 2. Lastly, the remaining base functions are cell-type and do not affect the conformity of the finite element.

The covariant Piola transformations maintain the conformity of the base functions across the mapping from the reference to the physical element [1,34] (see Appendix A). □

Remark 3.2. By employing the polynomial spaces $\mathcal{V}_i^{p-1}(\Gamma)$, $\mathcal{E}_{ij}^{p-1}(\Gamma)$ and $C_{123}^{p-1}(\Gamma)$ in the construction of the non-gradient base functions, one finds the $\mathcal{N}_{II}^{p}(\Gamma)$-element with a split between the kernel and non-kernel functions.

3.4. Raviart–Thomas

The Raviart–Thomas triangle element [27] enhances the Brezzi–Douglas–Marini triangle element by adding base functions not belonging to ker(div) such that $\mathrm{div}\,\mathcal{RT}^p = P^p$, thus improving convergence estimates for divergence terms. In order to construct Raviart–Thomas elements, one must split the polynomial basis between solenoidal and non-curl base functions. The construction follows the same lines as in Section 3.3.

The kernel of the space is partially given by curls of the $U^{p+1}(\Gamma)$ space without vertex base functions

$$\boldsymbol{\phi}_i(\xi,\eta) = \boldsymbol{R}\nabla_\xi n_i^{p+1}\,, \tag{3.31}$$

amounting to $(p+2)(p+1)/2-3$ base functions. Next the lowest order Raviart–Thomas $\mathcal{RT}^0(\Gamma)$ base functions [29] are added

$$\boldsymbol{\phi}_1^I = \begin{bmatrix} 1-\xi \\ -\eta \end{bmatrix}, \qquad \boldsymbol{\phi}_2^I = \begin{bmatrix} \xi \\ \eta - 1 \end{bmatrix}, \qquad \boldsymbol{\phi}_3^I = \begin{bmatrix} -\xi \\ -\eta \end{bmatrix}, \tag{3.32}$$

accounting for constant fields in $\mathbb{R}^2$ and mapping to constant fields in $\mathbb{R}$ via the divergence operator, $\mathrm{div}\,\mathcal{RT}^0(\Gamma) = \mathbb{R}$. We complete the space by introducing polytopal template sets for non-curl base functions composed of shifted and scaled linear source fields (see Fig. 14), centred around their respective polytopes

$$\begin{aligned} &\mathcal{T}_1 = \{-\boldsymbol{\phi}_3^I\}, && \mathcal{T}_2 = \{\boldsymbol{\phi}_2^I\}, && \mathcal{T}_{12} = \{\boldsymbol{\phi}_2^I - \boldsymbol{\phi}_3^I\}, \\ &\mathcal{T}_{13} = \{-\boldsymbol{\phi}_1^I - \boldsymbol{\phi}_3^I\}, && \mathcal{T}_{23} = \{\boldsymbol{\phi}_2^I - \boldsymbol{\phi}_1^I\}, && \mathcal{T}_{123} = \{\boldsymbol{\phi}_2^I - \boldsymbol{\phi}_1^I - \boldsymbol{\phi}_3^I\}, \end{aligned} \tag{3.33}$$

such that the entire template reads

$$\mathcal{T} = \{\mathcal{T}_1, \mathcal{T}_2, \mathcal{T}_{12}, \mathcal{T}_{13}, \mathcal{T}_{23}, \mathcal{T}_{123}\}. \tag{3.34}$$

With the template at hand we can construct the Raviart–Thomas element

$$\begin{aligned} &\mathcal{RT}^p(\Gamma) = \mathcal{RT}^0(\Gamma) \oplus \left\{ \bigoplus_{j\in\mathcal{J}} \boldsymbol{R}\nabla\mathcal{E}_j^{p+1}(\Gamma) \right\} \oplus \boldsymbol{R}\nabla C_{123}^{p+1}(\Gamma) \oplus \left\{ \bigoplus_{i=1}^{2} \mathcal{V}_i^p(\Gamma) \otimes \mathcal{T}_i \right\} \oplus \left\{ \bigoplus_{j\in\mathcal{J}} \mathcal{E}_j^p(\Gamma) \otimes \mathcal{T}_j \right\} \oplus \{C_{123}^p(\Gamma) \otimes \mathcal{T}_{123}\}, \\ &\mathcal{J} = \{(1,2),(1,3),(2,3)\}. \end{aligned} \tag{3.35}$$

Definition 3.5 (*Triangle $\mathcal{RT}^p$ Base Functions*)**.** The base functions of the triangle Raviart–Thomas element are defined on their respective polytope as follows.

- On each edge e_{ij} the base functions read

$$\text{Edge:} \qquad \boldsymbol{\phi}(\xi,\eta) = \boldsymbol{\phi}^I\,, \qquad \boldsymbol{\phi}^I \in \left\{ \boldsymbol{\phi} \in \mathcal{RT}^0 \mid \mathrm{tr}_n^{\parallel}\boldsymbol{\phi}\Big|_{e_{ij}} \neq 0 \right\}, \tag{3.36a}$$

$$\boldsymbol{\phi}(\xi,\eta) = \boldsymbol{R}\nabla_\xi n\,, \qquad n \in \mathcal{E}_{ij}^{p+1}\,, \tag{3.36b}$$

- The cell base functions are given by

$$\begin{aligned} &\text{Vertex-cell:} && \boldsymbol{\phi}(\xi,\eta) = n\ell\,, && n \in \mathcal{V}_1^p\,, && \ell \in \mathcal{T}_1\,, && (3.37a)\\ &&& \boldsymbol{\phi}(\xi,\eta) = n\ell\,, && n \in \mathcal{V}_2^p\,, && \ell \in \mathcal{T}_2\,, && (3.37b)\\ &\text{Edge-cell:} && \boldsymbol{\phi}(\xi,\eta) = n\ell\,, && n \in \mathcal{E}_{12}^p\,, && \ell \in \mathcal{T}_{12}\,, && (3.37c)\\ &&& \boldsymbol{\phi}(\xi,\eta) = n\ell\,, && n \in \mathcal{E}_{13}^p\,, && \ell \in \mathcal{T}_{13}\,, && (3.37d)\\ &&& \boldsymbol{\phi}(\xi,\eta) = n\ell\,, && n \in \mathcal{E}_{23}^p\,, && \ell \in \mathcal{T}_{23}\,, && (3.37e)\\ &\text{Cell:} && \boldsymbol{\phi}(\xi,\eta) = n\ell\,, && n \in C_{123}^p\,, && \ell \in \mathcal{T}_{123}\,, && (3.37f)\\ &&& \boldsymbol{\phi}(\xi,\eta) = \boldsymbol{R}\nabla_\xi n\,, && n \in C_{123}^{p+1}\,, && && (3.37g) \end{aligned}$$

such that their tangential trace vanishes on all edges.

Several cubic base functions are depicted in Fig. 15.

Theorem 3.7 (*Linear Independence*). *The set of base functions given by the lowest order Raviart–Thomas element, the curls of an $H^1(\Gamma)$-conforming polynomial subspace $U^{p+1}(\Gamma)$ (excluding vertex base functions) and the tensor product of the $U^p(\Gamma)$ base functions with the polytopal template yield a linearly independent polynomial basis for $\mathcal{RT}^p$.*

Proof. The proof follows the same lines as in Theorem 3.5. □

Theorem 3.8 ($H(\mathrm{div}, A)$-*conformity*). *The resulting finite element is $H(\mathrm{div}, A)$-conforming under contravariant Piola mappings.*

Proof. The lowest order Raviart–Thomas base functions are $H(\mathrm{div}, A)$-conforming due to their degrees of freedom. The curl base functions are conforming by exact sequence property $\boldsymbol{R}\nabla H^1(A) \subset H(\mathrm{div}, A)$, as depicted in Fig. 2. Finally, the remaining base functions are cell-type and as such, do not affect the conformity of the finite element.

The contravariant Piola transformations maintain the conformity of the base functions across the mapping from the reference to the physical element [1,34] (see Appendix A). □

Remark 3.3. By employing the polynomial spaces $\mathcal{V}_i^{p-1}(\Gamma)$, $\mathcal{E}_{ij}^{p-1}(\Gamma)$ and $C_{123}^{p-1}(\Gamma)$ in the construction of the non-curl base functions one finds the $\mathcal{BDM}^p(\Gamma)$-element with a split between the kernel and non-kernel functions.

4. Three-dimensional templates

This section is dedicated to the introduction of polytopal templates on the reference tetrahedron

$$\Omega = \{(\xi, \eta, \zeta) \in [0,1]^3 \mid \xi + \eta + \zeta \leq 1\}\,. \tag{4.1}$$

To that end, the tetrahedron is decomposed into its base polytopes given by its vertices $\{v_1, v_2, v_3, v_4\}$, its edges $\{e_{12}, e_{13}, e_{14}, e_{23}, e_{24}, e_{34}\}$, its faces $\{f_{123}, f_{124}, f_{134}, f_{234}\}$, and its cell c_{1234}, see Fig. 16. Further, each polytope is associated with base functions belonging to an $H^1(\Omega)$-conforming subspace $U^p(\Omega)$ with $\dim U^p(\Omega) = \dim P^p(\Omega) = (p+3)(p+2)(p+1)/6$, see for example Fig. 17.

Definition 4.1 (*Tetrahedron $U^p(\Omega)$-polytopal Spaces*). Each polytope is associated with a space of base functions as follows:

- Each vertex is associated with the space of its respective base function $\mathcal{V}_i^p(\Omega)$. As such, there are four spaces in total $i \in \{1,2,3,4\}$ and each one is of dimension one, $\dim \mathcal{V}_i^p(\Omega) = 1 \quad \forall\, i \in \{1,2,3,4\}$. The index p refers to the polynomial order of the space, which is always 1 if a hierarchical polynomial basis is employed.
- For each edge there exists a space of edge functions $\mathcal{E}_j^p(\Omega)$ with $j \in \mathcal{J} = \{(1,2),(1,3),(1,4),(2,3),(2,4),(3,4)\}$. The dimension of each edge space is given by $\dim \mathcal{E}_j^p(\Omega) = p-1$.
- For each face there exists a space of face base functions $\mathcal{F}_k^p(\Omega)$ with $k \in \mathcal{K} = \{(1,2,3),(1,2,4),(1,3,4),(2,3,4)\}$, where the dimension of the spaces reads $\dim \mathcal{F}_k^p(\Omega) = (p-2)(p-1)/2$.
- Lastly, the space of cell base function is given by $C_{1234}^p(\Omega)$ with the dimensionality $\dim C_{1234}^p(\Omega) = (p-3)(p-2)(p-1)/6$.

The association with a respective polytope is according to Definition 2.1 with respect to the trace operator for H^1.

We present polytopal templates for the construction of Nédélec elements of the second type and Brezzi–Douglas–Marini elements. For the formulation of Nédélec elements of the first type and Raviart–Thomas elements using Legendre polynomials see [34,35], or [36,37,40] for a Bernstein basis.

4.1. Nédélec II

We proceed analogously to the definition of the Nédélec element of the second type [25] for triangles by constructing a polytopal template on the unit tetrahedron. The template is then used in conjunction with an $H^1(\Omega)$-conforming polynomial basis to span the $\mathcal{N}_{II}(\Omega)$-space on the unit tetrahedron.

We define the vertex-edge tangent vector $\mathbf{e}_3$ for v_1–e_{12} such that its tangential projection is one on e_{12} and zero on all other neighbouring edges. The same vector is the tangent vector associated with edge e_{12}. Next we define the edge-face vector $-\mathbf{e}_2$ for the edge e_{12} and face f_{123}. On the face f_{123} we employ the base vectors $\mathbf{e}_3$ and $\mathbf{e}_2$ which span the plane on the face. Lastly, we employ the full set of the Cartesian base vectors for the cell, namely $\mathbf{e}_3$, $\mathbf{e}_2$ and $\mathbf{e}_1$. The template vectors of the remaining polytopes are derived by covariant Piola transformations of the unit tetrahedron c_{1234} to equivalent permutations c_{ijkl} and by adjusting the sign of the vector to ensure a positive projection on the tangent vector, analogous to Fig. 6. The resulting template is given by the super-set of the following polytopal sets depicted in Fig. 18

$$\mathcal{T}_1 = \{\mathbf{e}_3, \mathbf{e}_2, \mathbf{e}_1\}, \quad \mathcal{T}_2 = \{\mathbf{e}_1 + \mathbf{e}_2 + \mathbf{e}_3, \mathbf{e}_2, \mathbf{e}_1\}, \quad \mathcal{T}_3 = \{\mathbf{e}_1 + \mathbf{e}_2 + \mathbf{e}_3, -\mathbf{e}_3, \mathbf{e}_1\},$$
$$\mathcal{T}_4 = \{\mathbf{e}_1 + \mathbf{e}_2 + \mathbf{e}_3, -\mathbf{e}_3, -\mathbf{e}_2\}, \quad \mathcal{T}_{12} = \{\mathbf{e}_3, -\mathbf{e}_2, -\mathbf{e}_1\}, \quad \mathcal{T}_{13} = \{\mathbf{e}_2, \mathbf{e}_3, -\mathbf{e}_1\},$$
$$\mathcal{T}_{14} = \{\mathbf{e}_1, \mathbf{e}_3, \mathbf{e}_2\}, \quad \mathcal{T}_{23} = \{\mathbf{e}_2, \mathbf{e}_1 + \mathbf{e}_2 + \mathbf{e}_3, -\mathbf{e}_1\}, \quad \mathcal{T}_{24} = \{\mathbf{e}_1, \mathbf{e}_1 + \mathbf{e}_2 + \mathbf{e}_3, \mathbf{e}_2\},$$

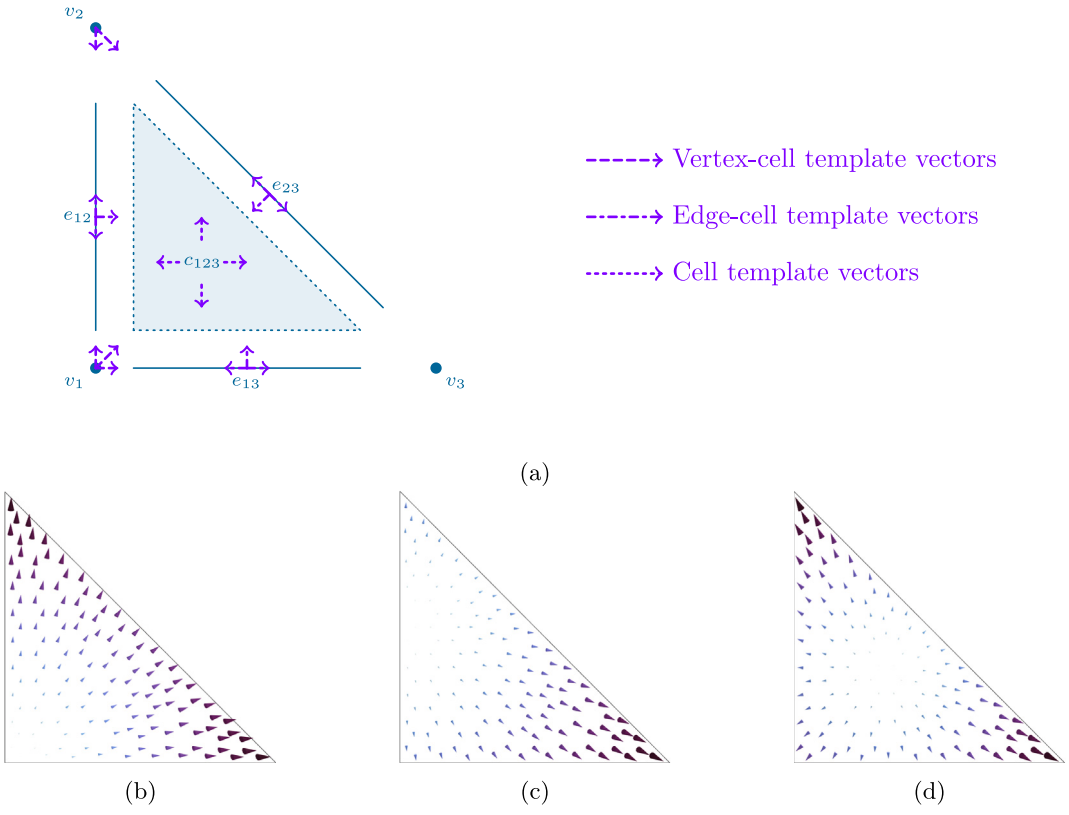

Fig. 14. Template vectors on the reference triangle for base functions orthogonal to the kernel of the div operator (a). The template of the first vertex (b), followed by the template of the first edge (c) and lastly, the cell template (d).

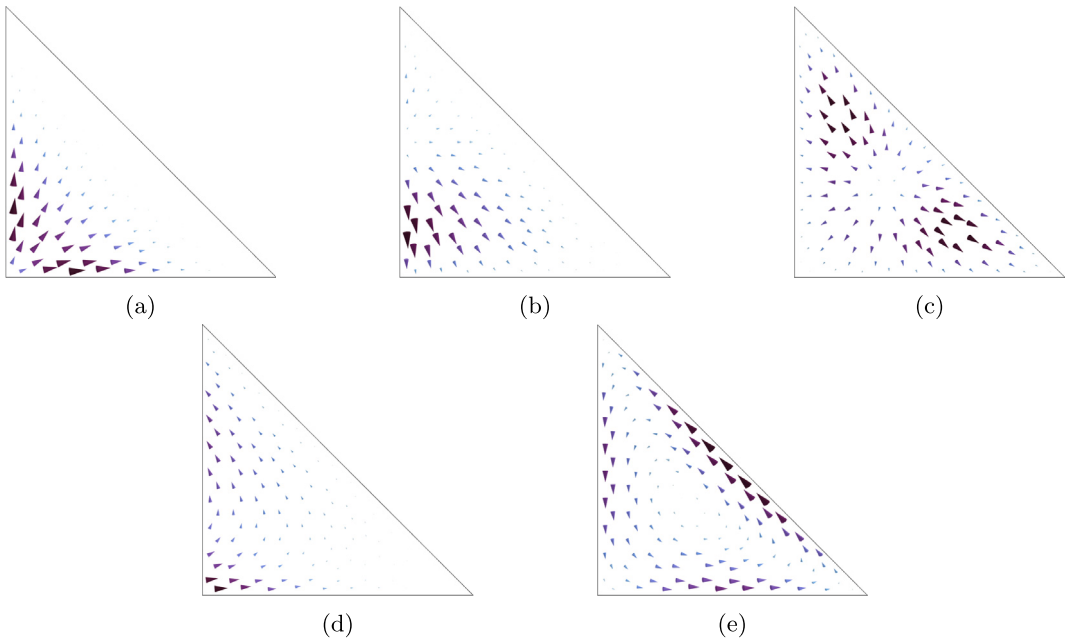

Fig. 15. Non-curl vertex-cell (a), edge-cell (b) and pure cell (c) base functions. Curl edge (d) and cell (e) base functions. The base functions belong to the triangle Raviart–Thomas element.

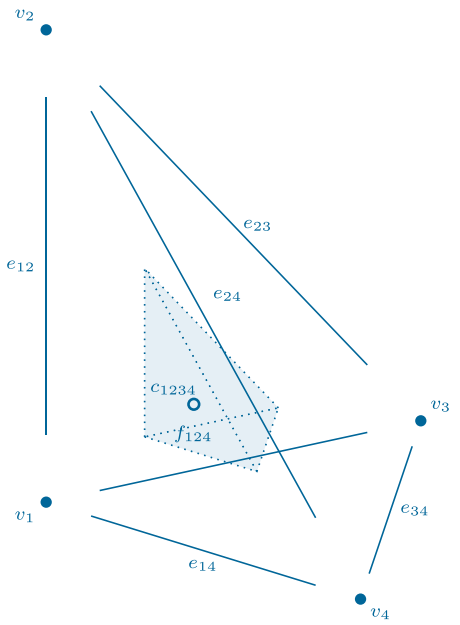

Fig. 16. Decomposition of the unit tetrahedron into vertices, edges, faces and the cell.

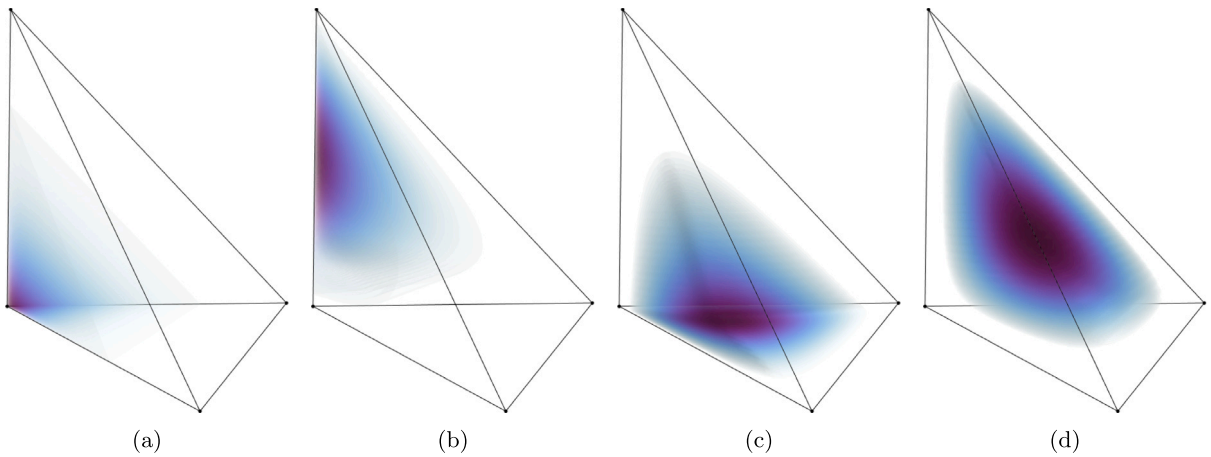

Fig. 17. Vertex (a), edge (b), face (c), and cell (c) base functions on the reference tetrahedron. Dark colours represent higher values of the field.

$$\begin{aligned}
&\mathcal{T}_{34} = \{\mathbf{e}_1, \mathbf{e}_1 + \mathbf{e}_2 + \mathbf{e}_3, -\mathbf{e}_3\}, && \mathcal{T}_{123} = \{\mathbf{e}_3, \mathbf{e}_2, -\mathbf{e}_1\}, && \mathcal{T}_{124} = \{\mathbf{e}_3, \mathbf{e}_1, \mathbf{e}_2\}, \\
&\mathcal{T}_{134} = \{\mathbf{e}_2, \mathbf{e}_1, -\mathbf{e}_3\}, && \mathcal{T}_{234} = \{\mathbf{e}_2, \mathbf{e}_1, \mathbf{e}_1 + \mathbf{e}_2 + \mathbf{e}_3\}, && \mathcal{T}_{1234} = \{\mathbf{e}_3, \mathbf{e}_2, \mathbf{e}_1\},
\end{aligned} \tag{4.2}$$

and reads

$$\mathcal{T} = \{\mathcal{T}_1, \mathcal{T}_2, \mathcal{T}_3, \mathcal{T}_4, \mathcal{T}_{12}, \mathcal{T}_{13}, \mathcal{T}_{14}, \mathcal{T}_{23}, \mathcal{T}_{24}, \mathcal{T}_{34}, \mathcal{T}_{123}, \mathcal{T}_{124}, \mathcal{T}_{134}, \mathcal{T}_{234}, \mathcal{T}_{1234}\}. \tag{4.3}$$

As such, we can define the Nédélec element of the second type with the polytopal template and an underlying subspace $U^p(\Omega) \subset H^1(\Omega)$

$$\begin{aligned}
&\mathcal{N}^p_{II}(\Omega) = \left\{\bigoplus_{i=1}^{4} \mathcal{V}^p_i(\Omega) \otimes \mathcal{T}_i\right\} \oplus \left\{\bigoplus_{j\in\mathcal{J}} \mathcal{E}^p_j(\Omega) \otimes \mathcal{T}_j\right\} \oplus \left\{\bigoplus_{k\in\mathcal{K}} \mathcal{F}^p_k(\Omega) \otimes \mathcal{T}_k\right\} \oplus \{C^p_{1234}(\Omega) \otimes \mathcal{T}_{1234}\}, \\
&\mathcal{J} = \{(1,2),(1,3),(1,4),(2,3),(2,4),(3,4)\}, \qquad \mathcal{K} = \{(1,2,3),(1,2,4),(1,3,4),(2,3,4)\},
\end{aligned} \tag{4.4}$$

where $\mathcal{V}^p_i(\Omega)$ are the sets of vertex base functions, $\mathcal{E}^p_j(\Omega)$ are the sets of edge base functions, $\mathcal{F}^p_k(\Omega)$ are the sets of face base functions and $C^p_{1234}(\Omega)$ is the set of cell base functions.

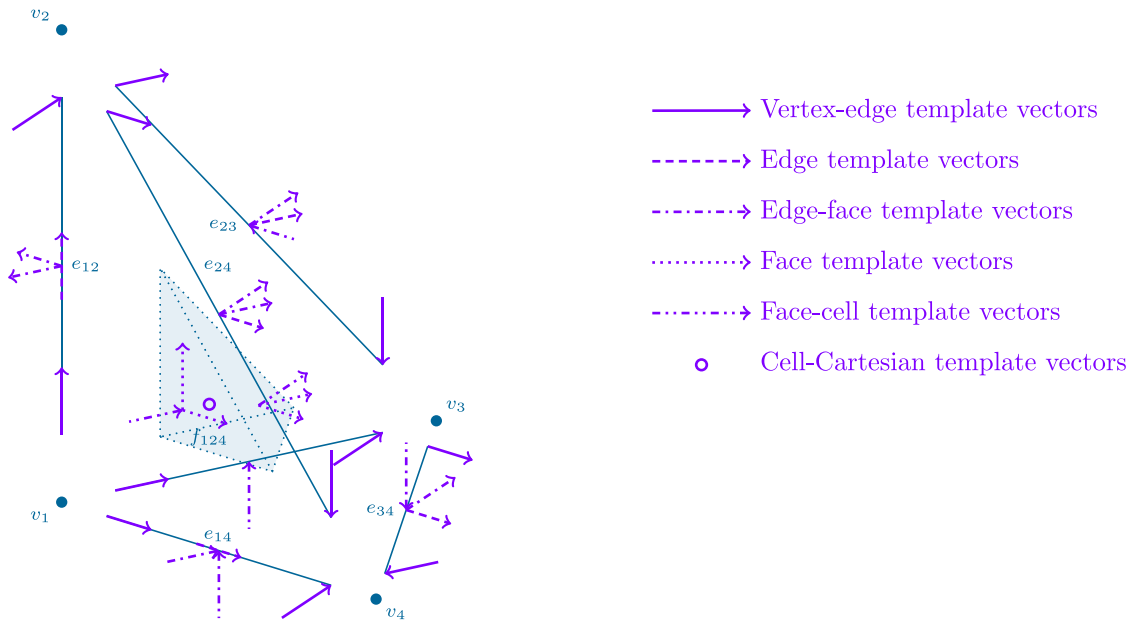

Fig. 18. Template vectors for the reference tetrahedron on their corresponding polytopes. Only vectors on the visible sides of the tetrahedron are depicted. The template allows to construct Nédélec elements of the second type.

Definition 4.2 (*Tetrahedron $\mathcal{N}_{II}^p$ Base Functions*)**.** The base functions of the tetrahedral Nédélec element of the second type are defined on their respective polytopes as follows.

- On each edge e_{ij} with vertices v_i and v_j, the base functions read

$$\text{Vertex-edge:} \quad \vartheta(\xi,\eta,\zeta) = n\boldsymbol{\ell}\,, \quad n \in \mathcal{V}_i^p\,, \quad \boldsymbol{\ell} \in \left\{ \boldsymbol{\ell} \in \mathcal{T}_i \mid \operatorname{tr}_t^{\parallel}\boldsymbol{\ell}\Big|_{e_{ij}} \neq 0 \right\}, \tag{4.5a}$$

$$\vartheta(\xi,\eta,\zeta) = n\boldsymbol{\ell}\,, \quad n \in \mathcal{V}_j^p\,, \quad \boldsymbol{\ell} \in \left\{ \boldsymbol{\ell} \in \mathcal{T}_j \mid \operatorname{tr}_t^{\parallel}\boldsymbol{\ell}\Big|_{e_{ij}} \neq 0 \right\}, \tag{4.5b}$$

$$\text{Edge:} \quad \vartheta(\xi,\eta,\zeta) = n\boldsymbol{\ell}\,, \quad n \in \mathcal{E}_{ij}^p\,, \quad \boldsymbol{\ell} \in \left\{ \boldsymbol{\ell} \in \mathcal{T}_{ij} \mid \operatorname{tr}_t^{\parallel}\boldsymbol{\ell}\Big|_{e_{ij}} \neq 0 \right\}, \tag{4.5c}$$

  such that $\boldsymbol{\ell}$ is an element of the template sets, whose tangential trace does not vanish on the edge.
- For each face f_{ijk} with edges e_{ij}, e_{ik} and e_{jk} the base functions read

$$\text{Edge-face:} \quad \vartheta(\xi,\eta,\zeta) = n\boldsymbol{\ell}\,, \quad n \in \mathcal{E}_{ij}^p\,, \quad \boldsymbol{\ell} \in \left\{ \boldsymbol{\ell} \in \mathcal{T}_{ij} \mid \operatorname{tr}_t^{\parallel}\boldsymbol{\ell}\Big|_{e_{ij}} = 0\,, \quad \operatorname{tr}_n^{\perp}\boldsymbol{\ell}\Big|_{f_{ijk}} \neq 0 \right\}, \tag{4.6a}$$

$$\vartheta(\xi,\eta,\zeta) = n\boldsymbol{\ell}\,, \quad n \in \mathcal{E}_{ik}^p\,, \quad \boldsymbol{\ell} \in \left\{ \boldsymbol{\ell} \in \mathcal{T}_{ik} \mid \operatorname{tr}_t^{\parallel}\boldsymbol{\ell}\Big|_{e_{ik}} = 0\,, \quad \operatorname{tr}_n^{\perp}\boldsymbol{\ell}\Big|_{f_{ijk}} \neq 0 \right\}, \tag{4.6b}$$

$$\vartheta(\xi,\eta,\zeta) = n\boldsymbol{\ell}\,, \quad n \in \mathcal{E}_{jk}^p\,, \quad \boldsymbol{\ell} \in \left\{ \boldsymbol{\ell} \in \mathcal{T}_{jk} \mid \operatorname{tr}_t^{\parallel}\boldsymbol{\ell}\Big|_{e_{jk}} = 0\,, \quad \operatorname{tr}_n^{\perp}\boldsymbol{\ell}\Big|_{f_{ijk}} \neq 0 \right\}, \tag{4.6c}$$

$$\text{Face:} \quad \vartheta(\xi,\eta,\zeta) = n\boldsymbol{\ell}\,, \quad n \in C_{ijk}^p\,, \quad \boldsymbol{\ell} \in \left\{ \boldsymbol{\ell} \in \mathcal{T}_{ijk} \mid \operatorname{tr}_n^{\perp}\boldsymbol{\ell}\Big|_{f_{ijk}} \neq 0 \right\}. \tag{4.6d}$$

  such that their tangential trace vanishes on all edges.
- The cell base functions read

$$\text{Face-cell:} \quad \vartheta(\xi,\eta,\zeta) = n\boldsymbol{\ell}\,, \quad n \in C_{123}^p\,, \quad \boldsymbol{\ell} \in \left\{ \boldsymbol{\ell} \in \mathcal{T}_{123} \mid \operatorname{tr}_n^{\perp}\boldsymbol{\ell}\Big|_{f_{123}} = 0 \right\}, \tag{4.7a}$$

$$\vartheta(\xi,\eta,\zeta) = n\boldsymbol{\ell}\,, \quad n \in C_{124}^p\,, \quad \boldsymbol{\ell} \in \left\{ \boldsymbol{\ell} \in \mathcal{T}_{124} \mid \operatorname{tr}_n^{\perp}\boldsymbol{\ell}\Big|_{f_{124}} = 0 \right\}, \tag{4.7b}$$

$$\vartheta(\xi,\eta,\zeta) = n\boldsymbol{\ell}\,, \quad n \in C_{134}^p\,, \quad \boldsymbol{\ell} \in \left\{ \boldsymbol{\ell} \in \mathcal{T}_{134} \mid \operatorname{tr}_n^{\perp}\boldsymbol{\ell}\Big|_{f_{134}} = 0 \right\}, \tag{4.7c}$$

$$\vartheta(\xi,\eta,\zeta) = n\mathscr{t}\,, \qquad n \in C^p_{234}\,, \qquad \mathscr{t} \in \left\{ \mathscr{t} \in \mathcal{T}_{234} \mid \mathrm{tr}^{\perp}_{n}\mathscr{t}\Big|_{f_{234}} = 0 \right\}, \tag{4.7d}$$

Cell: $$\vartheta(\xi,\eta,\zeta) = n\mathscr{t}\,, \qquad n \in C^p_{1234}\,, \qquad \mathscr{t} \in \mathcal{T}_{1234}\,. \tag{4.7e}$$

A depiction of the base functions is given in Fig. 19.

Theorem 4.1 (*Linear Independence*). *Let $U^p(\Omega)$ span an $H^1(\Omega)$-conforming basis on the unit tetrahedron, then its tensor product with the polytopal template yields a linearly independent basis for the Nédélec element of the second type $\mathcal{N}^p_{II}(\Omega)$.*

Proof. Linear independence of the vectorial base functions is inherited from the linear independence of the underlying $H^1(\Omega)$-conforming basis since each base function is multiplied with three linearly independent template vectors. Further, the dimension of the basis

$$\dim[U^p(\Omega)]^3 = \dim[P^p(\Omega)]^3 = \dim \mathcal{N}^p_{II}(\Omega)\,, \tag{4.8}$$

agrees with the dimension of the Nédélec element of the second type. □

Theorem 4.2 ($H(\mathrm{curl}, V)$-*conformity*). *Under covariant Piola transformations, the basis spans an $H(\mathrm{curl}, V)$-conforming subspace.*

Proof. The conformity of a grid composed solely of unit tetrahedrons is $H(\mathrm{curl}, V)$-conforming due to the methodology used to construct the polytopal template, namely by an initial definition of a minimal set of template vectors and permutations of the unit tetrahedron, such that the jump condition on the interface of neighbouring elements V_i and V_j reduces from $[\![\mathrm{tr}^{\perp}_{n}\mathbf{u}]\!]|_{\Xi_{ij}} = 0$ to $[\![\mathrm{tr}\,\langle \mathbf{t}, \mathbf{u}\rangle]\!]|_{\Xi_{ij}} = c_{ij}(n_i - n_j)$ of the tangential components of the non-cell base functions. The latter is satisfied by the underlying $U^p(V)$-space. Conformity of a general grid is consequently achieved by employing covariant Piola transformations, as the tangential projection is maintained [1,34] (see Appendix A) (see Fig. 19). □

4.2. Brezzi-Douglas-Marini

The last element we consider is the Brezzi–Douglas–Marini element [26] on the unit tetrahedron. We start the construction by defining a single vertex-face vector for the vertex v_1 and the face f_{123}, namely $-\mathbf{e}_1$. Next we define two template vectors on the edge e_{12}. The vector $-\mathbf{e}_1$ is associated with the face f_{123} and the vector $\mathbf{e}_3$ is an edge-cell vector. On the face introduce the template $\{-\mathbf{e}_1, \mathbf{e}_3, \mathbf{e}_2\}$, where the first vector is associated with the face and the last two are face-cell vectors. Lastly, we employ the Cartesian basis in the cell c_{1234}. The template vectors for the remaining polytopes are computed by permutations of the unit tetrahedron c_{ijkl} with the contravariant Piola transformation, compare with Fig. 6. The complete template is depicted in Fig. 20, where the polytopal template sets read

$$\begin{aligned}
&\mathcal{T}_1 = \{-\mathbf{e}_1, \mathbf{e}_2, -\mathbf{e}_3\}\,, && \mathcal{T}_2 = \{\mathbf{e}_3 - \mathbf{e}_1, \mathbf{e}_2 - \mathbf{e}_3, -\mathbf{e}_3\}\,, && \mathcal{T}_3 = \{\mathbf{e}_2 - \mathbf{e}_1, \mathbf{e}_2 - \mathbf{e}_3, -\mathbf{e}_2\}\,,\\
&\mathcal{T}_4 = \{\mathbf{e}_2 - \mathbf{e}_1, \mathbf{e}_1 - \mathbf{e}_3, -\mathbf{e}_1\}\,, && \mathcal{T}_{12} = \{-\mathbf{e}_1, \mathbf{e}_2, \mathbf{e}_3\}\,, && \mathcal{T}_{13} = \{-\mathbf{e}_1, -\mathbf{e}_3, \mathbf{e}_2\}\,,\\
&\mathcal{T}_{14} = \{\mathbf{e}_2, -\mathbf{e}_3, \mathbf{e}_1\}\,, && \mathcal{T}_{23} = \{\mathbf{e}_3 - \mathbf{e}_1, -\mathbf{e}_3, \mathbf{e}_2 - \mathbf{e}_3\}\,, && \mathcal{T}_{24} = \{\mathbf{e}_2 - \mathbf{e}_3, -\mathbf{e}_3, \mathbf{e}_1 - \mathbf{e}_3\}\,,\\
&\mathcal{T}_{34} = \{\mathbf{e}_2 - \mathbf{e}_3, -\mathbf{e}_2, \mathbf{e}_1 - \mathbf{e}_2\}\,, && \mathcal{T}_{123} = \{-\mathbf{e}_1, \mathbf{e}_3, \mathbf{e}_2\}\,, && \mathcal{T}_{124} = \{\mathbf{e}_2, \mathbf{e}_3, \mathbf{e}_1\}\,,\\
&\mathcal{T}_{134} = \{-\mathbf{e}_3, \mathbf{e}_2, \mathbf{e}_1\}\,, && \mathcal{T}_{234} = \{-\mathbf{e}_3, \mathbf{e}_2 - \mathbf{e}_3, \mathbf{e}_1 - \mathbf{e}_3\}\,, && \mathcal{T}_{1234} = \{\mathbf{e}_3, \mathbf{e}_2, \mathbf{e}_1\}\,.
\end{aligned} \tag{4.9}$$

The super-set is given by

$$\mathcal{T} = \{\mathcal{T}_1, \mathcal{T}_2, \mathcal{T}_3, \mathcal{T}_4, \mathcal{T}_{12}, \mathcal{T}_{13}, \mathcal{T}_{14}, \mathcal{T}_{23}, \mathcal{T}_{24}, \mathcal{T}_{34}, \mathcal{T}_{123}, \mathcal{T}_{124}, \mathcal{T}_{134}, \mathcal{T}_{234}, \mathcal{T}_{1234}\}\,. \tag{4.10}$$

With the template at hand, we define the $\mathcal{BDM}^p(\Omega)$-element using an underlying U^p subspace by tensor products

$$\begin{aligned}
&\mathcal{BDM}^p(\Omega) = \left\{ \bigoplus_{i=1}^{4} \mathcal{V}^p_i(\Omega) \otimes \mathcal{T}_i \right\} \oplus \left\{ \bigoplus_{j\in\mathcal{J}} \mathcal{E}^p_j(\Omega) \otimes \mathcal{T}_j \right\} \oplus \left\{ \bigoplus_{k\in\mathcal{K}} \mathcal{F}^p_k(\Omega) \otimes \mathcal{T}_k \right\} \oplus \{C^p_{1234}(\Omega) \otimes \mathcal{T}_{1234}\}\,,\\
&\mathcal{J} = \{(1,2),(1,3),(1,4),(2,3),(2,4),(3,4)\}\,, \qquad \mathcal{K} = \{(1,2,3),(1,2,4),(1,3,4),(2,3,4)\}\,,
\end{aligned} \tag{4.11}$$

where $\mathcal{V}^p_i(\Omega)$ are the sets of vertex base functions, $\mathcal{E}^p_j(\Omega)$ are the sets of edge base functions, $\mathcal{F}^p_k(\Omega)$ are the sets of face base functions and $C^p_{1234}(\Omega)$ is the set of cell base functions.

Definition 4.3 (*Tetrahedron $\mathcal{BDM}^p$ Base Functions*). The base functions of the tetrahedral Brezzi–Douglas–Marini element are defined on their respective polytope as follows.

- For each face f_{ijk} with vertices v_i, v_j and v_k, and edges e_{ij}, e_{ik} and e_{jk} the base functions read

Vertex-face: $$\boldsymbol{\phi}(\xi,\eta,\zeta) = n\mathscr{t}\,, \qquad n \in \mathcal{V}^p_i\,, \qquad \mathscr{t} \in \left\{ \mathscr{t} \in \mathcal{T}_i \mid \mathrm{tr}^{\parallel}_{n}\mathscr{t}\Big|_{f_{ijk}} \neq 0 \right\}, \tag{4.12a}$$

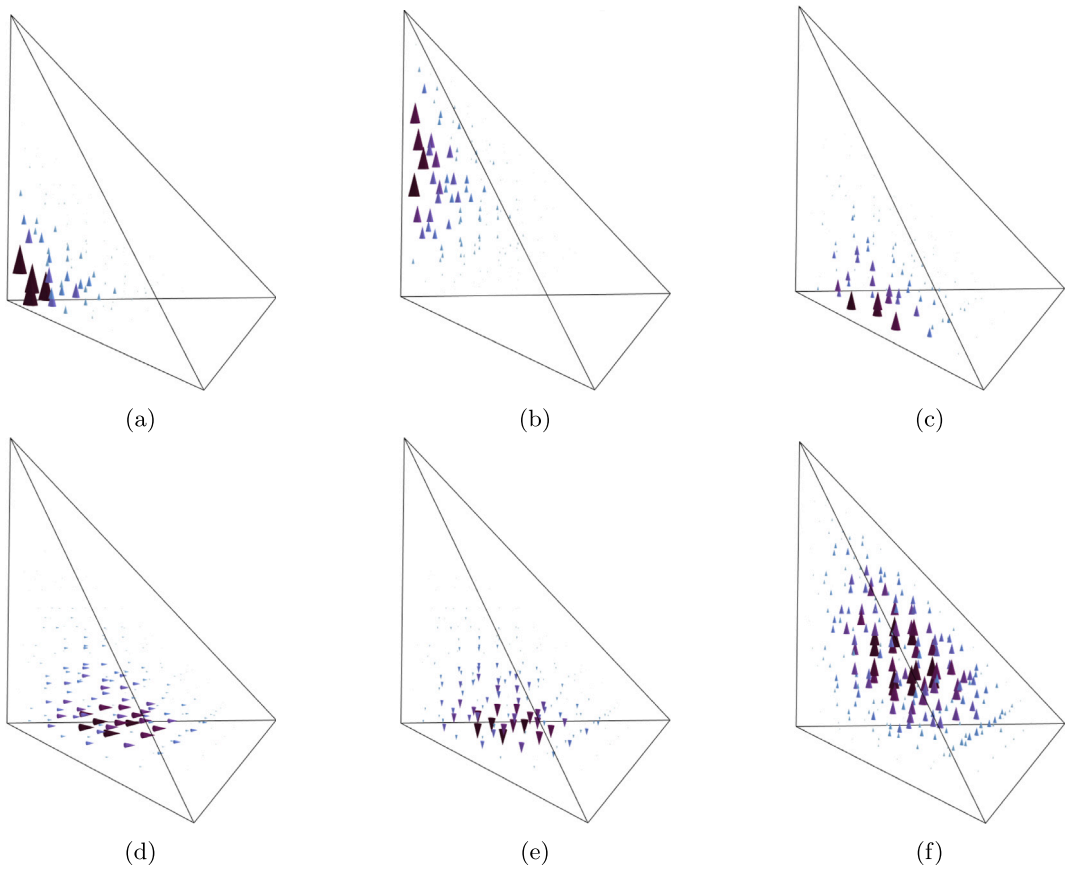

Fig. 19. Quartic vertex-edge (a) and edge (b) base functions on e_{12}, edge-face (c) base function on e_{14} for f_{124}, face (d) and face-cell (e) base functions on f_{134}, and pure cell (f) base functions of the Nédélec element of the second type on the reference tetrahedron.

$$\boldsymbol{\phi}(\xi,\eta,\zeta) = n\boldsymbol{\ell}\,, \qquad n \in \mathcal{V}_j^p\,, \qquad \boldsymbol{\ell} \in \left\{ \boldsymbol{\ell} \in \mathcal{T}_j \mid \mathrm{tr}_n^{\parallel}\boldsymbol{\ell}\Big|_{f_{ijk}} \neq 0 \right\}, \tag{4.12b}$$

$$\boldsymbol{\phi}(\xi,\eta,\zeta) = n\boldsymbol{\ell}\,, \qquad n \in \mathcal{V}_k^p\,, \qquad \boldsymbol{\ell} \in \left\{ \boldsymbol{\ell} \in \mathcal{T}_k \mid \mathrm{tr}_n^{\parallel}\boldsymbol{\ell}\Big|_{f_{ijk}} \neq 0 \right\}, \tag{4.12c}$$

Edge-face:
$$\boldsymbol{\phi}(\xi,\eta,\zeta) = n\boldsymbol{\ell}\,, \qquad n \in \mathcal{E}_{ij}^p\,, \qquad \boldsymbol{\ell} \in \left\{ \boldsymbol{\ell} \in \mathcal{T}_{ij} \mid \mathrm{tr}_n^{\parallel}\boldsymbol{\ell}\Big|_{f_{ijk}} \neq 0 \right\}, \tag{4.12d}$$

$$\boldsymbol{\phi}(\xi,\eta,\zeta) = n\boldsymbol{\ell}\,, \qquad n \in \mathcal{E}_{ik}^p\,, \qquad \boldsymbol{\ell} \in \left\{ \boldsymbol{\ell} \in \mathcal{T}_{ik} \mid \mathrm{tr}_n^{\parallel}\boldsymbol{\ell}\Big|_{f_{ijk}} \neq 0 \right\}, \tag{4.12e}$$

$$\boldsymbol{\phi}(\xi,\eta,\zeta) = n\boldsymbol{\ell}\,, \qquad n \in \mathcal{E}_{jk}^p\,, \qquad \boldsymbol{\ell} \in \left\{ \boldsymbol{\ell} \in \mathcal{T}_{jk} \mid \mathrm{tr}_n^{\parallel}\boldsymbol{\ell}\Big|_{f_{ijk}} \neq 0 \right\}, \tag{4.12f}$$

Face:
$$\boldsymbol{\phi}(\xi,\eta,\zeta) = n\boldsymbol{\ell}\,, \qquad n \in C_{ijk}^p\,, \qquad \boldsymbol{\ell} \in \left\{ \boldsymbol{\ell} \in \mathcal{T}_{ijk} \mid \mathrm{tr}_n^{\parallel}\boldsymbol{\ell}\Big|_{f_{ijk}} \neq 0 \right\}. \tag{4.12g}$$

such that their tangential trace vanishes on all edges.

- The cell base functions read

Edge-cell:
$$\boldsymbol{\phi}(\xi,\eta,\zeta) = n\boldsymbol{\ell}\,, \qquad n \in \mathcal{E}_{12}^p\,, \qquad \boldsymbol{\ell} \in \left\{ \boldsymbol{\ell} \in \mathcal{T}_{12} \mid \mathrm{tr}_n^{\parallel}\boldsymbol{\ell}\Big|_{f_{123}} = 0\,, \quad \mathrm{tr}_n^{\parallel}\boldsymbol{\ell}\Big|_{f_{124}} = 0 \right\}, \tag{4.13a}$$

$$\boldsymbol{\phi}(\xi,\eta,\zeta) = n\boldsymbol{\ell}\,, \qquad n \in \mathcal{E}_{13}^p\,, \qquad \boldsymbol{\ell} \in \left\{ \boldsymbol{\ell} \in \mathcal{T}_{13} \mid \mathrm{tr}_n^{\parallel}\boldsymbol{\ell}\Big|_{f_{123}} = 0\,, \quad \mathrm{tr}_n^{\parallel}\boldsymbol{\ell}\Big|_{f_{134}} = 0 \right\}, \tag{4.13b}$$

$$\boldsymbol{\phi}(\xi,\eta,\zeta) = n\boldsymbol{\ell}\,, \qquad n \in \mathcal{E}_{14}^p\,, \qquad \boldsymbol{\ell} \in \left\{ \boldsymbol{\ell} \in \mathcal{T}_{14} \mid \mathrm{tr}_n^{\parallel}\boldsymbol{\ell}\Big|_{f_{124}} = 0\,, \quad \mathrm{tr}_n^{\parallel}\boldsymbol{\ell}\Big|_{f_{134}} = 0 \right\}, \tag{4.13c}$$

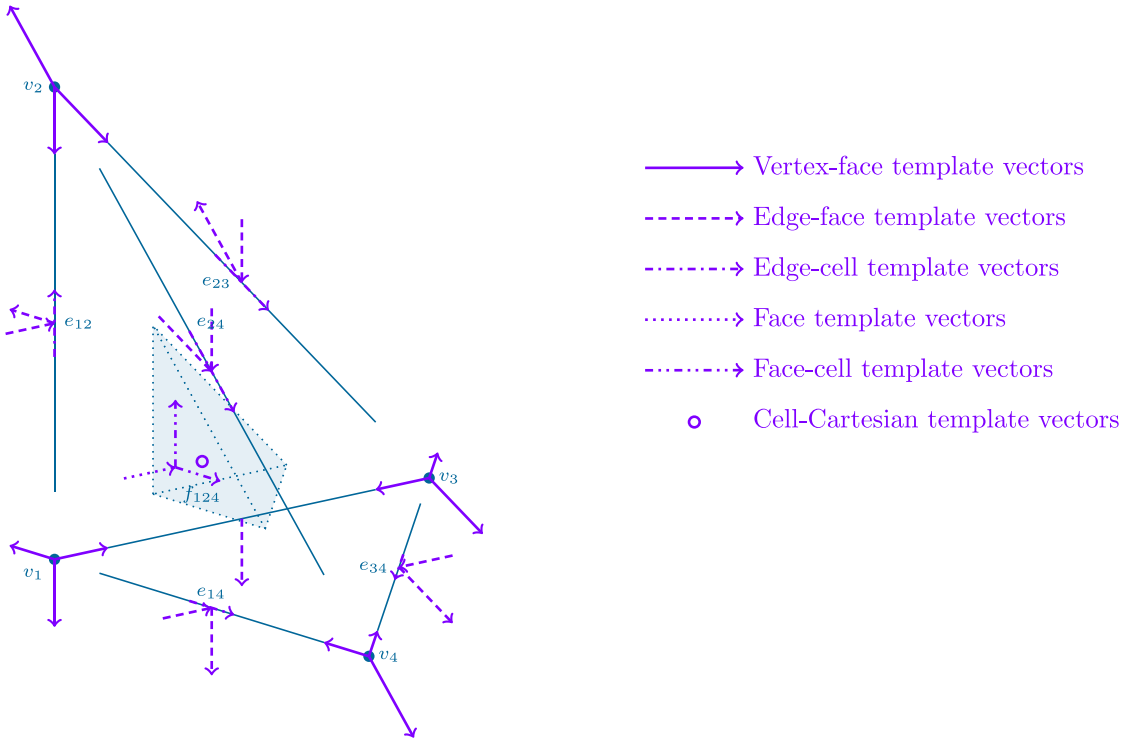

Fig. 20. Template vectors for the reference tetrahedron on their corresponding polytopes. Only vectors on the visible sides of the tetrahedron are depicted. The template is associated with the Brezzi–Douglas–Marini element.

$$\boldsymbol{\phi}(\xi,\eta,\zeta) = n\mathscr{C}\,, \qquad n \in \mathcal{E}^p_{23}\,, \qquad \mathscr{C} \in \left\{ \mathscr{C} \in \mathcal{T}_{23} \mid \mathrm{tr}^{\parallel}_n \mathscr{C}\Big|_{f_{123}} = 0\,, \quad \mathrm{tr}^{\parallel}_n \mathscr{C}\Big|_{f_{234}} = 0 \right\}, \tag{4.13d}$$

$$\boldsymbol{\phi}(\xi,\eta,\zeta) = n\mathscr{C}\,, \qquad n \in \mathcal{E}^p_{24}\,, \qquad \mathscr{C} \in \left\{ \mathscr{C} \in \mathcal{T}_{24} \mid \mathrm{tr}^{\parallel}_n \mathscr{C}\Big|_{f_{124}} = 0\,, \quad \mathrm{tr}^{\parallel}_n \mathscr{C}\Big|_{f_{234}} = 0 \right\}, \tag{4.13e}$$

$$\boldsymbol{\phi}(\xi,\eta,\zeta) = n\mathscr{C}\,, \qquad n \in \mathcal{E}^p_{34}\,, \qquad \mathscr{C} \in \left\{ \mathscr{C} \in \mathcal{T}_{34} \mid \mathrm{tr}^{\parallel}_n \mathscr{C}\Big|_{f_{134}} = 0\,, \quad \mathrm{tr}^{\parallel}_n \mathscr{C}\Big|_{f_{234}} = 0 \right\}, \tag{4.13f}$$

Face-cell:

$$\boldsymbol{\phi}(\xi,\eta,\zeta) = n\mathscr{C}\,, \qquad n \in C^p_{123}\,, \qquad \mathscr{C} \in \left\{ \mathscr{C} \in \mathcal{T}_{123} \mid \mathrm{tr}^{\parallel}_n \mathscr{C}\Big|_{f_{123}} = 0 \right\}, \tag{4.13g}$$

$$\boldsymbol{\phi}(\xi,\eta,\zeta) = n\mathscr{C}\,, \qquad n \in C^p_{124}\,, \qquad \mathscr{C} \in \left\{ \mathscr{C} \in \mathcal{T}_{124} \mid \mathrm{tr}^{\parallel}_n \mathscr{C}\Big|_{f_{124}} = 0 \right\}, \tag{4.13h}$$

$$\boldsymbol{\phi}(\xi,\eta,\zeta) = n\mathscr{C}\,, \qquad n \in C^p_{134}\,, \qquad \mathscr{C} \in \left\{ \mathscr{C} \in \mathcal{T}_{134} \mid \mathrm{tr}^{\parallel}_n \mathscr{C}\Big|_{f_{134}} = 0 \right\}, \tag{4.13i}$$

$$\boldsymbol{\phi}(\xi,\eta,\zeta) = n\mathscr{C}\,, \qquad n \in C^p_{234}\,, \qquad \mathscr{C} \in \left\{ \mathscr{C} \in \mathcal{T}_{234} \mid \mathrm{tr}^{\parallel}_n \mathscr{C}\Big|_{f_{234}} = 0 \right\}, \tag{4.13j}$$

Cell:

$$\boldsymbol{\phi}(\xi,\eta,\zeta) = n\mathscr{C}\,, \qquad n \in C^p_{1234}\,, \qquad \mathscr{C} \in \mathcal{T}_{1234}\,, \tag{4.13k}$$

A depiction of the base functions is given in Fig. 21.

Theorem 4.3 (*Linear Independence*)**.** *Let $U^p(\Omega)$ be a polynomial $H^1(\Omega)$-conforming subspace on the unit tetrahedron, then its tensor product with the polytopal template yields a linearly independent basis for the Brezzi–Douglas–Marini element $\mathcal{BDM}^p(\Omega)$.*

Proof. Each base function from $U^p(\Omega)$ is multiplied with three linearly independent vectors, such that linear Independence is inherited on the vectorial level. □

Theorem 4.4 ($H(\mathrm{div}, V)$*-conformity*)**.** *Under contravariant Piola transformations, the basis spans an $H(\mathrm{div}, V)$-conforming subspace.*

Proof. The proof follows the same lines as in Theorem 4.2. The base functions are designed with the property

$$\langle \boldsymbol{\nu}, \boldsymbol{\phi}_i \rangle = n_i\,, \tag{4.14}$$

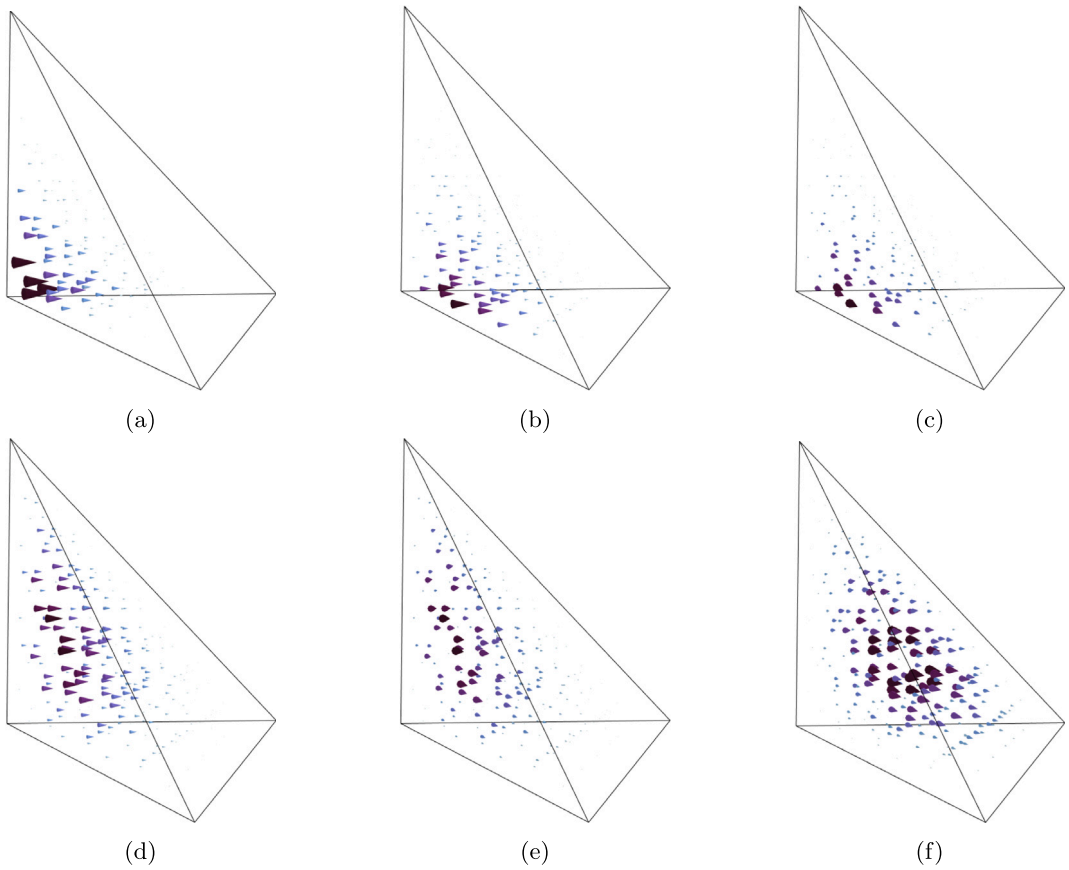

Fig. 21. Quartic vertex-face (a), edge-face (b), edge-cell (c), face (d), face-cell (e) and pure cell (f) base functions of the Brezzi–Douglas–Marini element on the reference tetrahedron. The face functions are associated with the face f_{124}.

for the normal components of the non-cell base functions, such that the trace interface condition is reduced to $[\![\mathrm{tr}\,\langle \mathbf{n}, \mathbf{u}\rangle]\!]|_{\Xi_{ij}} = c_{ij}(n_i - n_j) = 0$ from $[\![\mathrm{tr}_n^{\|}\mathbf{u}]\!]|_{\Xi_{ij}} = 0$, which is satisfied by the underlying $U^p(V)$ subspace. □

Remark 4.1. Note that unlike the two-dimensional version of the Brezzi–Douglas–Marini element on the triangle $\mathcal{BDM}^p(\Gamma)$, the three-dimensional version on the tetrahedron $\mathcal{BDM}^p(\Omega)$ cannot be constructed by rotating the base functions of the Nédélec element of the second type $\mathcal{N}_{II}^p(\Omega)$.

5. Examples

In the following we present two examples using Nédélec elements and the relaxed micromorphic model. The decay in the error is measured in the Lebesgue norm

$$\|\widetilde{u} - u^h\|_{L^2} = \sqrt{\int_V \|\widetilde{u} - u^h\|^2 \mathrm{d}V}\,, \tag{5.1}$$

in which context $\widetilde{u}$ is the analytical solution and u^h is the finite element approximation.

5.1. Relaxed micromorphic model of antiplane shear

The strong from of the relaxed micromorphic model of antiplane shear [30] reads

$$-\mu_{\mathrm{e}}\mathrm{div}\,(\nabla u - \mathbf{p}) = f \qquad \text{in} \quad A\,, \tag{5.2a}$$

$$-\mu_{\mathrm{e}}(\nabla u - \mathbf{p}) + \mu_{\mathrm{micro}}\,\mathbf{p} + \mu_{\mathrm{macro}}\,L_{\mathrm{c}}^2\,\boldsymbol{R}\nabla\mathrm{div}(\boldsymbol{R}\,\mathbf{p}) = \mathbf{m} \qquad \text{in} \quad A\,, \tag{5.2b}$$

$$u = \widetilde{u} \qquad \text{on} \quad s_D^u\,, \tag{5.2c}$$

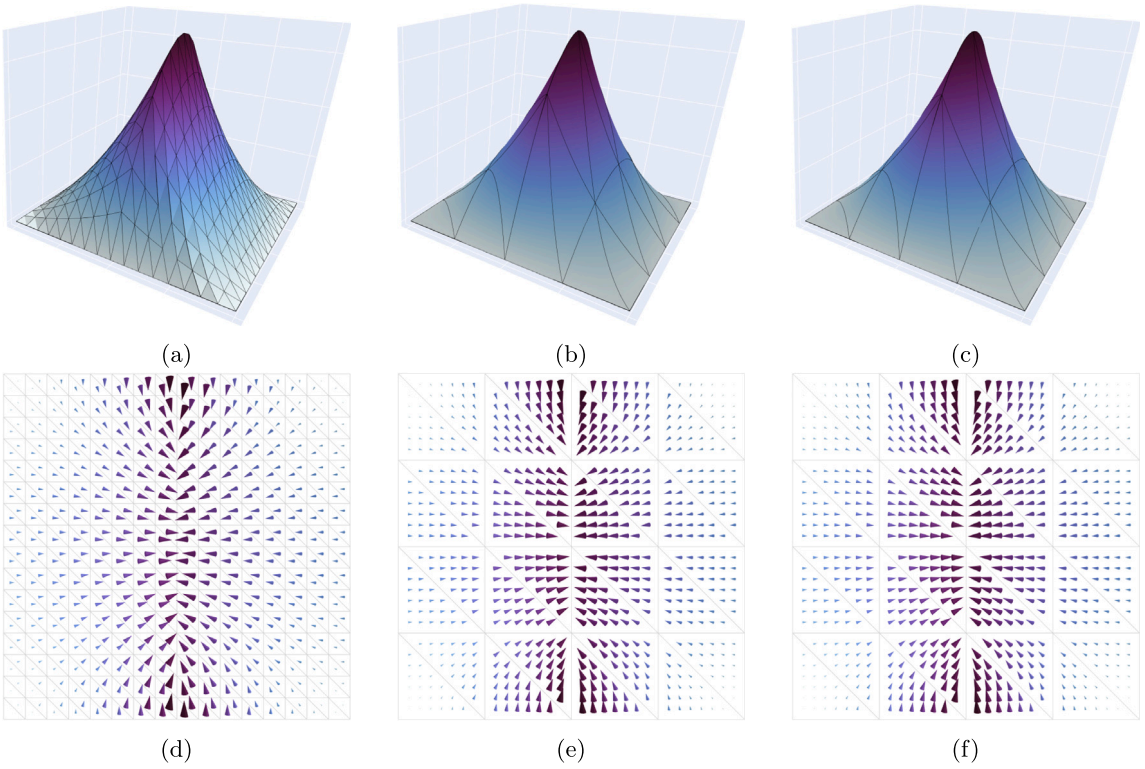

Fig. 22. Displacement field using 1090 linear elements (a), 32 quadratic elements (b) and 32 cubic elements (c), corresponding to 1090, 258, and 530 degrees of freedom, respectively. The related microdistortion fields are depicted in (d)–(f).

$$\langle \mathbf{p},\, \mathbf{t}\rangle = \langle \widetilde{\mathbf{p}},\, \mathbf{t}\rangle \qquad \text{on} \quad s_D^P\,, \tag{5.2d}$$

$$\langle \nabla u,\, \mathbf{n}\rangle = \langle \mathbf{p},\, \mathbf{n}\rangle \qquad \text{on} \quad s_N^u\,, \tag{5.2e}$$

$$\operatorname{div}(\boldsymbol{R}\,\mathbf{p}) = 0 \qquad \text{on} \quad s_N^P\,, \tag{5.2f}$$

where u is the antiplane displacement field, $\mathbf{p}$ is the microdistortion, $\mu_{\mathrm{e}}, \mu_{\mathrm{micro}}, \mu_{\mathrm{macro}}$ are shear material parameters and L_{c} is the characteristic length scale parameter. Body forces and micro-moments are given by f and $\boldsymbol{M}$, respectively. The corresponding bilinear and linear forms are given by

$$a(\{\delta u, \delta\mathbf{p}\}, \{u, \mathbf{p}\}) = \int_A \mu_{\mathrm{e}}\langle \nabla\delta u - \delta\mathbf{p},\, \nabla u - \mathbf{p}\rangle + \mu_{\mathrm{micro}}\langle \delta\mathbf{p},\, \mathbf{p}\rangle + \mu_{\mathrm{macro}} L_{\mathrm{c}}^2 \operatorname{div}(\boldsymbol{R}\,\delta\mathbf{p})\operatorname{div}(\boldsymbol{R}\,\mathbf{p})\,\mathrm{d}A\,, \tag{5.3a}$$

$$l(\{\delta u, \delta\mathbf{p}\}) = \int_A \delta u\, f + \langle \delta\mathbf{p},\, \mathbf{m}\rangle\,\mathrm{d}A\,. \tag{5.3b}$$

The problem is uniquely solvable for the space $X(A) = H^1(A) \times H(\mathrm{curl}, A)$ [30].

We set the material constants to $\mu_{\mathrm{e}} = \mu_{\mathrm{micro}} = \mu_{\mathrm{macro}} = L_{\mathrm{c}} = 1$ and prescribe an analytical solution by inserting predefined displacement and microdistortion fields

$$\widetilde{u} = \begin{cases} (1-y^2)(e^{x+1}-1) & \text{for} \quad x \le 0 \\ (1-y^2)(e^{1-x}-1) & \text{for} \quad x > 0 \end{cases}, \qquad \widetilde{\mathbf{p}} = \nabla\widetilde{u} = \begin{cases} \begin{bmatrix} \left(1-y^2\right) e^{x+1} \\ 2y\left(1-e^{x+1}\right) \end{bmatrix} & \text{for} \quad x \le 0 \\ \begin{bmatrix} \left(y^2-1\right) e^{1-x} \\ 2y\left(1-e^{1-x}\right) \end{bmatrix} & \text{for} \quad x > 0 \end{cases}. \tag{5.4}$$

into the strong form Eqs. (5.2a) and (5.2b), such that the corresponding right-hand-side reads

$$f = 0\,, \qquad \mathbf{m} = \begin{cases} \begin{bmatrix} \left(1-y^2\right) e^{x+1} \\ 2y\left(1-e^{x+1}\right) \end{bmatrix} & \text{for} \quad x \le 0 \\ \begin{bmatrix} \left(y^2-1\right) e^{1-x} \\ 2y\left(e^{x}-e\right) e^{-x} \end{bmatrix} & \text{for} \quad x > 0 \end{cases}. \tag{5.5}$$

The prescribed solution Eq. (5.4) is the analytical solution for the boundary conditions

$$u\Big|_{\partial A} = \widetilde{u}\,, \langle \mathbf{p},\, \mathbf{t}\rangle\Big|_{\partial A} = \langle \widetilde{\mathbf{p}},\, \mathbf{t}\rangle\,, \tag{5.6}$$

such that $s_D = \partial A$, since the solution is unique. Clearly, the displacement field u is $C^0(A)$-continuous and its gradient is solely tangentially continuous, such that Nédélec elements are required for optimal convergence results.

We demonstrate the behaviour of the elements constructed using linear and quadratic Lagrangian $\mathcal{L}$, and cubic Bernstein $\mathcal{B}$ polynomials. The solution of the displacement and microdistortion fields is depicted in Fig. 22. The difference between the quadratic and cubic displacement fields is subtle but can be observed by the sharp form of the solution at $(x, y) = (0, 0)$. As shown in Fig. 23, the elements yield optimal convergence rates and correctly capture the discontinuity of the normal component of the microdistortion. This is also visible in the depiction of the fields in Fig. 22. In comparison, a formulation with $\mathbf{p} \in [H^1(A)]^2$ would impose the higher regularity $C^0(A)$ on the microdistortion. This can be done using $H^1(A)$-conforming finite elements for the formulation of the microdistortion $\mathbf{p}$ and leads to sub-optimal convergence rates, see [30].

5.2. Three-dimensional relaxed micromorphic continuum

The balance equations of the relaxed micromorphic continuum [11] are given by

$$-\mathrm{Div}\,[\mathbb{C}_e \mathrm{sym}\,(\mathrm{D}\mathbf{u} - \boldsymbol{P}) + \mathbb{C}_c \mathrm{skew}\,(\mathrm{D}\mathbf{u} - \boldsymbol{P})] = \mathbf{f} \qquad \text{in} \quad V\,, \tag{5.7a}$$

$$-\mathbb{C}_e \mathrm{sym}\,(\mathrm{D}\mathbf{u} - \boldsymbol{P}) - \mathbb{C}_c \mathrm{skew}\,(\mathrm{D}\mathbf{u} - \boldsymbol{P}) + \mathbb{C}_{\mathrm{micro}} \mathrm{sym}\,\boldsymbol{P} + \mu_{\mathrm{macro}}\, L_c^2 \mathrm{Curl}\,\mathrm{Curl}\,\boldsymbol{P} = \boldsymbol{M} \qquad \text{in} \quad V\,, \tag{5.7b}$$

$$\mathbf{u} = \widetilde{\mathbf{u}} \qquad \text{on} \quad A_D^u\,, \tag{5.7c}$$

$$\boldsymbol{P} \times \mathbf{n} = \widetilde{\boldsymbol{P}} \times \mathbf{n} \qquad \text{on} \quad A_D^P\,, \tag{5.7d}$$

$$[\mathbb{C}_e \mathrm{sym}\,(\mathrm{D}\mathbf{u} - \boldsymbol{P}) + \mathbb{C}_c \mathrm{skew}\,(\mathrm{D}\mathbf{u} - \boldsymbol{P})]\,\mathbf{n} = 0 \qquad \text{on} \quad A_N^u\,, \tag{5.7e}$$

$$\mathrm{Curl}\,\boldsymbol{P} \times \mathbf{n} = 0 \qquad \text{on} \quad A_N^P\,. \tag{5.7f}$$

where $\mathbf{u}$ is a three-dimensional displacement field, $\boldsymbol{P}$ is second order tensor field for the microdistortion, $\mathbb{C}_e, \mathbb{C}_{\mathrm{micro}}$ are standard fourth order elasticity tensors, $\mathbb{C}_c$ is a rotational coupling tensor for infinitesimal rotations, μ_{macro} is the macroscopic shear modulus and L_c is the characteristic length scale parameter. The body forces $\mathbf{f}$ and micro-moments $\boldsymbol{M}$ are now given by a three-dimensional vector a second order tensor, respectively. Further, the gradient $\mathrm{D}(\cdot)$ and $\mathrm{Curl}\,(\cdot)$ operators are constructed by applying the standard operators row-wise. The bilinear form reads

$$\begin{aligned} a(\{\delta\mathbf{u}, \delta\boldsymbol{P}\}, \{\mathbf{u}, \boldsymbol{P}\}) = \int_V & \langle \mathrm{sym}\,(\mathrm{D}\delta\mathbf{u} - \delta\boldsymbol{P}),\, \mathbb{C}_e \mathrm{sym}\,(\mathrm{D}\mathbf{u} - \boldsymbol{P})\rangle + \langle \mathrm{sym}\,\delta\boldsymbol{P},\, \mathbb{C}_{\mathrm{micro}} \mathrm{sym}\,\boldsymbol{P}\rangle \\ & + \langle \mathrm{skew}\,(\mathrm{D}\delta\mathbf{u} - \delta\boldsymbol{P}),\, \mathbb{C}_c \mathrm{skew}\,(\mathrm{D}\mathbf{u} - \boldsymbol{P})\rangle + \mu_{\mathrm{macro}} L_c^2 \langle \mathrm{Curl}\,\delta\boldsymbol{P},\, \mathrm{Curl}\,\boldsymbol{P}\rangle\,\mathrm{d}V\,, \end{aligned} \tag{5.8}$$

and the corresponding linear form is given by

$$l(\{\delta\mathbf{u}, \delta\boldsymbol{P}\}) = \int_V \langle \delta\mathbf{u},\, \mathbf{f}\rangle + \langle \delta\boldsymbol{P},\, \boldsymbol{M}\rangle\,\mathrm{d}V\,. \tag{5.9}$$

The problem is well-posed in $X(V) = [H^1(V)]^3 \times [H(\mathrm{curl}, V)]^3$ due to the generalized Korn-type inequalities [49–55], compare with [12,31,56,57].

We define the material constants $\lambda_e = \mu_e = \lambda_{\mathrm{micro}} = \mu_{\mathrm{micro}} = \mu_{\mathrm{macro}} = L_c = 1$ and $\mu_c = 0$ and prescribe the solution

$$\widetilde{\mathbf{u}} = \begin{bmatrix} 0 \\ 0 \\ \sin(\pi x) \end{bmatrix}, \widetilde{\boldsymbol{P}} = \mathrm{D}\widetilde{\mathbf{u}} + 10(1 - y^2)(1 - z^2)\sin(\pi x) \begin{bmatrix} 0 & 0 & 0 \\ 0 & 0 & 0 \\ 0 & -z & y \end{bmatrix}, \tag{5.10}$$

for which the right-hand-side reads

$$\mathbf{f} = \begin{bmatrix} 10\pi y(y^2 - 1)(z^2 - 1)\cos(\pi x) \\ 20(-y^2 + z^2)\sin(\pi x) \\ yz(60y^2 - 20z^2 - 40)\sin(\pi x) \end{bmatrix},$$

$$\boldsymbol{M} = \begin{bmatrix} 20y\left(y^2 - 1\right)\left(z^2 - 1\right)\sin(\pi x) & 0 & \cdots \\ 0 & 20y\left(y^2 - 1\right)\left(z^2 - 1\right)\sin(\pi x) & \\ \pi\left(20y^3 z - 20yz^3 + 1\right)\cos(\pi x) & z\left(120y^2 - 10\pi^2\left(y^2 - 1\right)\left(z^2 - 1\right) - 20\left(y^2 - 1\right)\left(z^2 - 1\right) - 80\right)\sin(\pi x) & \\ \cdots & \pi\cos(\pi x) & \\ & -20z\left(y^2 - 1\right)\left(z^2 - 1\right)\sin(\pi x) & \\ & y\left(-120z^2 + 60\left(y^2 - 1\right)\left(z^2 - 1\right) + 10\pi^2\left(y^2 - 1\right)\left(z^2 - 1\right) + 80\right)\sin(\pi x) & \end{bmatrix}. \tag{5.11}$$

We set the boundary $A_D = \partial V$, such that the prescribed solution corresponds with the analytical solution due to uniqueness.

A depiction of the approximation is given in Fig. 24. In order to capture the wave-shaped solution, either a fine grid or higher order elements are needed. The convergence rates shown in Fig. 25 are optimal. Although the initial solution of the quadratic element on the coarse grid seems well enough, it is simply due to the fortunate placing of element interfaces at the peaks and cannot be expected in general discretizations. All discretizations converge at an optimal rate, compare [31].

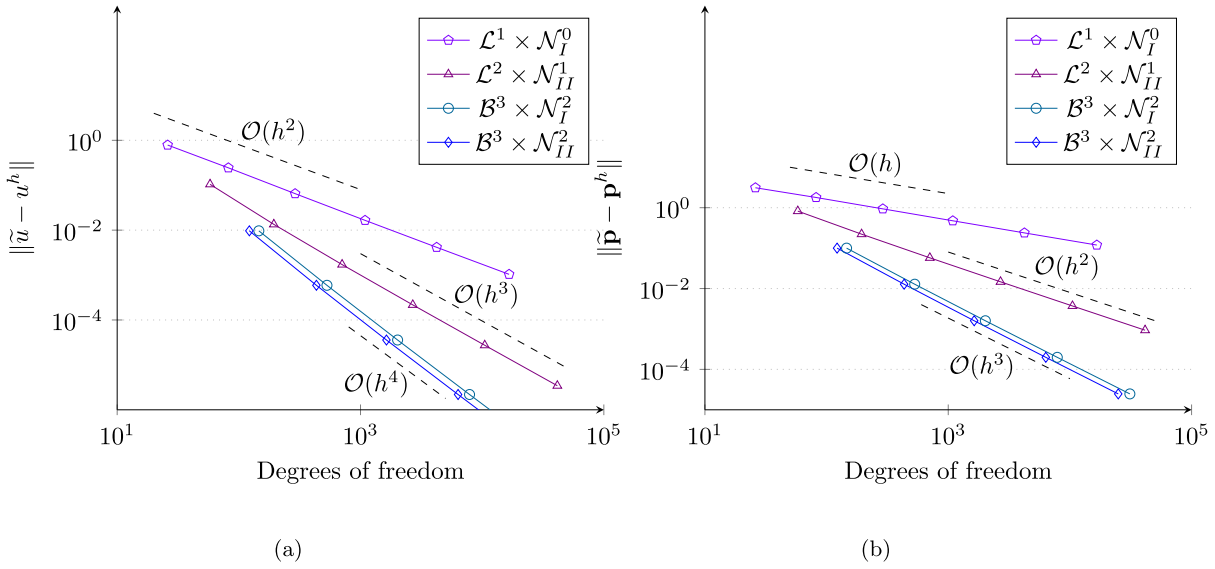

Fig. 23. Displacement (a) and microdistortion (b) fields of the discontinuous-normal problem and convergence rates under h-refinement (b).

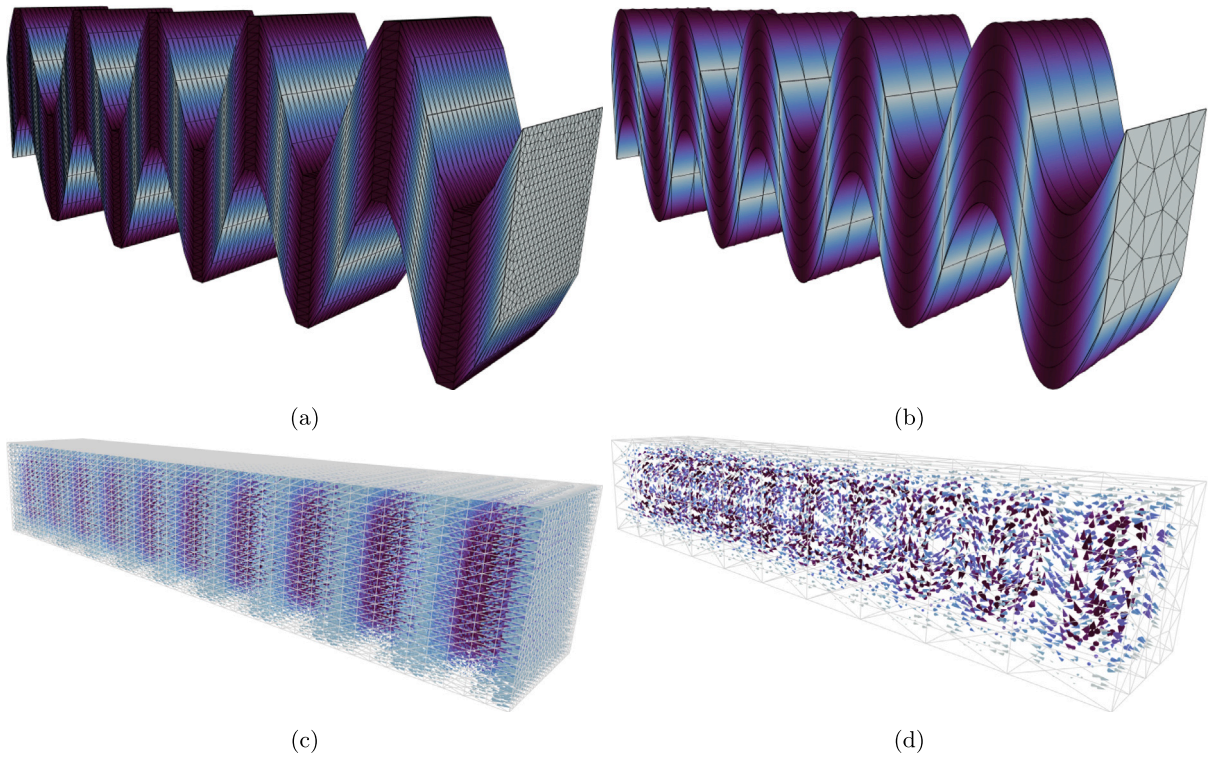

Fig. 24. Depiction of the displacement field (a), (c) and the last row of the microdistortion field (b), (d) for 141900 linear elements corresponding to 597820 degrees of freedom and 1260 cubic elements corresponding to 96358 degrees of freedom.

6. Conclusions and outlook

In this work we presented a novel method of constructing base functions for the spaces $H(\mathrm{curl})$ and $H(\mathrm{div})$ on the reference triangle and tetrahedron. The ability of the method to generate viable bases is proven by linear independence and conformity theorems. Further, the validity of the construction is demonstrated by two examples of the relaxed micromorphic model using Lagrange and Bernstein base functions for the formulation. As such, we conclude that the method can be used to generate $H(\mathrm{curl})$-

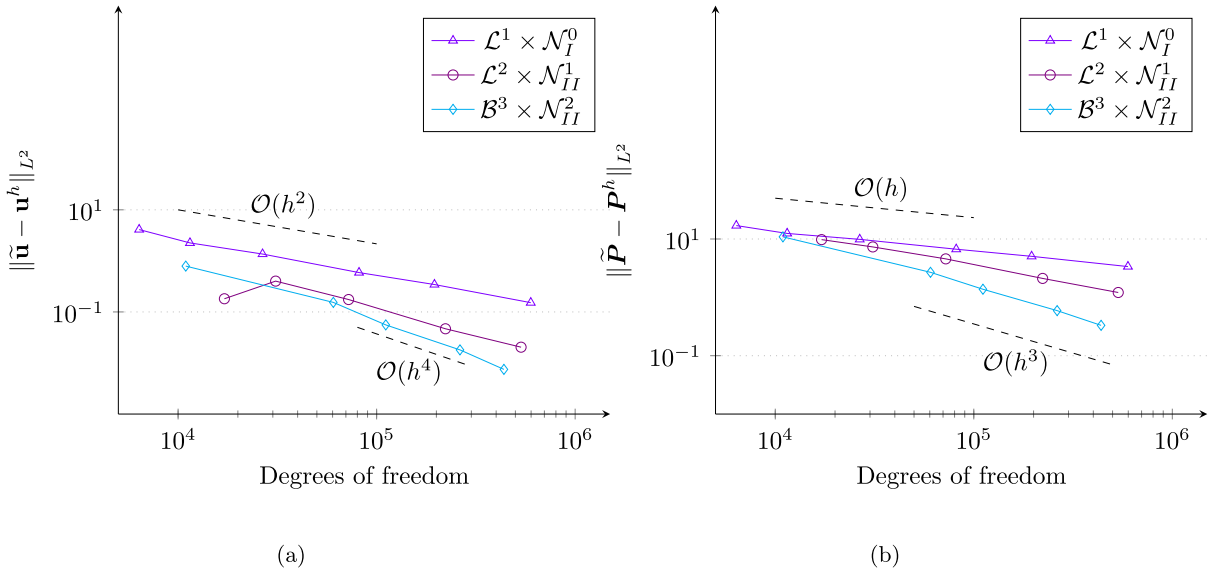

Fig. 25. Convergence under h-adaption for various polynomial orders.

and $H(\mathrm{div})$-conforming subspaces for a variety of H^1-conforming polynomial subspaces. The simplicity of the method makes its application straight-forward in the formulation of arbitrary order vectorial finite elements, as one must simply employ a higher order H^1-conforming subspace in the construction. Further, by construction, the vectorial basis can inherit characteristics of the underlying scalar basis. For example, the Kronecker delta property of Lagrange polynomials as demonstrated in the embedding of boundary conditions in [31], or the optimal complexity of Bernstein polynomials [58].

The vectorial polytopal templates presented in this work can be easily used to construct tensor-valued templates for tensor-valued finite elements, such as Regge [59,60] and Hellan–Herrman–Johnson [61]. These constructions will be made available in a future publication. This work did not discuss alternative reference elements, such as quads, prisms, pyramids or hexahedra. Further, the definition of Raviart–Thomas and Nédélec elements of the first type on the reference tetrahedron has not been addressed. The latter are topics for future works.

CRediT authorship contribution statement

Adam Sky: Writing – original draft, Visualization, Validation, Software, Methodology, Investigation, Conceptualization. **Ingo Muench:** Writing – review & editing, Supervision.

Declaration of competing interest

The authors declare that they have no known competing financial interests or personal relationships that could have appeared to influence the work reported in this paper.

Data availability

No data was used for the research described in the article.

Appendix A. Piola transformations

Consistent transformations are employed to map the base functions from the reference element to the physical element [1]. Effectively, every element in the physical domain is constructed from one reference element. If the mapping of the physical space is affine and achieved via barycentric functions for each element, the polynomial degree is maintained across transformations.

Scalar base functions transform according to

$$n(\mathbf{x}) = n \circ [\mathbf{x}^{-1}(\boldsymbol{\xi})] \,, \nabla_x n = \boldsymbol{J}^{-T} \nabla_\xi n \,, \tag{A.1}$$

where the result concerning the Jacobi matrix is a direct consequence of the chain rule.

Nédélec elements are defined via their action on the tangent vectors of the element. Consequently, a consistent transformation is given by the equality

$$\langle \boldsymbol{\theta}, \mathbf{t} \rangle \mathrm{d}s = \langle \boldsymbol{\theta}, \mathrm{d}\mathbf{s} \rangle = \langle \boldsymbol{\theta}, \boldsymbol{J}\mathrm{d}\boldsymbol{\mu} \rangle = \langle \boldsymbol{\vartheta}, \mathrm{d}\boldsymbol{\mu} \rangle = \langle \boldsymbol{\vartheta}, \boldsymbol{\tau} \rangle \mathrm{d}\mu \quad \Longleftrightarrow \quad \boldsymbol{\theta} = \boldsymbol{J}^{-T} \boldsymbol{\vartheta} \,, \tag{A.2}$$

known as the covariant Piola transformation. This is the same transformation as for gradients, thus respecting the commuting property Fig. 2. Further, vectors undergoing the latter transformation exhibit the following transformation of the curl operator

$$\mathrm{curl}_x \boldsymbol{\theta} = \nabla_x \times \boldsymbol{\theta} = (\boldsymbol{J}^{-T}\nabla_\xi) \times (\boldsymbol{J}^{-T}\boldsymbol{\vartheta}) = \mathrm{cof}\,(\boldsymbol{J}^{-T})(\nabla_\xi \times \boldsymbol{\vartheta}) = \frac{1}{\det \boldsymbol{J}}\boldsymbol{J}\,\mathrm{curl}_\xi \boldsymbol{\vartheta}\,, \tag{A.3}$$

being the so called contravariant Piola transformation. The result is won by observing that

$$\nabla_x \times \boldsymbol{J}^{-T} = \nabla_x \times \nabla_x \boldsymbol{\xi} = 0\,. \tag{A.4}$$

For two-dimensional domains the formula reduces to

$$\mathrm{div}_x(\boldsymbol{R}\boldsymbol{\theta}) = \frac{1}{\det \boldsymbol{J}}\mathrm{div}_\xi(\boldsymbol{R}\boldsymbol{\vartheta})\,, \tag{A.5}$$

since the curl operator produces a scalar. The contravariant Piola transformation is compatible with the commuting diagram and preserves normal projections on the element's boundary. To see this characteristic define the base function $\boldsymbol{\phi}$ in the reference domain and $\boldsymbol{\varphi}$ in the physical domain and equate their normal projections on the outer surface of both domains

$$\langle \boldsymbol{\varphi}, \mathbf{n}\rangle \mathrm{d}A = \langle \boldsymbol{\varphi}, \mathrm{d}\mathbf{A}\rangle = \langle \boldsymbol{\varphi}, \mathrm{cof}\,(\boldsymbol{J})\mathrm{d}\boldsymbol{\Gamma}\rangle = \langle \boldsymbol{\phi}, \mathrm{d}\boldsymbol{\Gamma}\rangle = \langle \boldsymbol{\phi}, \boldsymbol{\nu}\rangle \mathrm{d}\Gamma \quad \Longleftrightarrow \quad \boldsymbol{\varphi} = \frac{1}{\det \boldsymbol{J}}\boldsymbol{J}\boldsymbol{\phi}\,. \tag{A.6}$$

The divergence of functions mapped by a contravariant Piola transformation is given by

$$\begin{aligned}
\int_V q\,\mathrm{div}_x \boldsymbol{\varphi}\,\mathrm{d}V &= \oint_{\partial V} q\,\langle \boldsymbol{\varphi}, \mathbf{n}\rangle\,\mathrm{d}A - \int_V \langle \nabla_x q, \boldsymbol{\varphi}\rangle\,\mathrm{d}V \\
&= \oint_{\partial\Omega} \hat{q}\,\langle \frac{1}{\det \boldsymbol{J}}\boldsymbol{J}\boldsymbol{\phi}, \det(\boldsymbol{J})\,\boldsymbol{J}^{-T}\boldsymbol{\nu}\rangle\,\mathrm{d}\Gamma - \int_\Omega \langle \boldsymbol{J}^{-T}\nabla_\xi \hat{q}, \frac{1}{\det \boldsymbol{J}}\boldsymbol{J}\boldsymbol{\phi}\rangle\,\det \boldsymbol{J}\,\mathrm{d}\Omega \\
&= \oint_{\partial\Omega} \hat{q}\,\langle \boldsymbol{\phi}, \boldsymbol{\nu}\rangle\,\mathrm{d}\Gamma - \int_\Omega \langle \nabla_\xi \hat{q}, \boldsymbol{\phi}\rangle\,\mathrm{d}\Omega \\
&= \int_\Omega \hat{q}\,\mathrm{div}_\xi \boldsymbol{\phi}\,\mathrm{d}\Omega = \int_V q\,\mathrm{div}_\xi(\boldsymbol{\phi})\,\frac{1}{\det \boldsymbol{J}}\mathrm{d}V \qquad \forall\, q \in C^\infty(\overline{V})\,,
\end{aligned} \tag{A.7}$$

where $\hat{q} = q \circ \mathbf{x}$. Consequently, there holds

$$\mathrm{div}_x \boldsymbol{\varphi} = \frac{1}{\det \boldsymbol{J}}\,\mathrm{div}_\xi \boldsymbol{\phi}\,. \tag{A.8}$$

Appendix B. Consistent orientations

The co- and contravariant Piola transformations are not enough to ensure a consistent orientation of tangential or normal projections on edges and faces of neighbouring elements. The transformations control the size of the projections, but not whether these are parallel or anti-parallel with respect to the projection of neighbouring elements at the interface. However, consistent projections is a key requirement in ensuring no jumps occur in the trace of the respective space. In this work we rely on a solution based on the sequencing of vertices and the separation of orientational data, directly in the construction. We define the following rule for the orientation of edges

$$e_{ij} = \{v_i, v_j\} \qquad \text{s.t.} \quad i < j\,. \tag{B.1}$$

This means each edge starts at the lower vertex index and ends at the higher vertex index. This definition determines the orientation of the edge tangent vector, see Fig. 26. Analogously, for faces we define

$$f_{ijk} = \{v_i, v_j, v_k\} \qquad \text{s.t.} \quad i < j < k\,, \tag{B.2}$$

such that each face is given by a sequence of increasing vertex indices. The orientation of the surface normal is given according to the left-hand rule. In other words, the direction of the normal is determined by the cross product of the vectors arising from the edges $\{v_i, v_j\}$ and $\{v_i, v_k\}$

$$\mathbf{n}_{ijk} \parallel \mathbf{t}_{ij} \times \mathbf{t}_{ik}\,. \tag{B.3}$$

Consequently, in order to map each triangle (in 2D) or tetrahedron (in 3D) in the mesh to this orientation, we define each element as an increasing vertex-index sequence

$$T = \{v_i, v_j, v_k, v_l\} \qquad \text{s.t.} \quad i < j < k < l\,, \tag{B.4}$$

as depicted in Fig. 26. The latter ensures the consistent projections of the base functions, since they are all mapped from the same reference element. However, integration in the reference element is determined by the determinant of the Jacobi matrix

$$\int_{V_e} \mathrm{d}V = \int_\Omega \det \boldsymbol{J}\,\mathrm{d}\Omega\,, \tag{B.5}$$

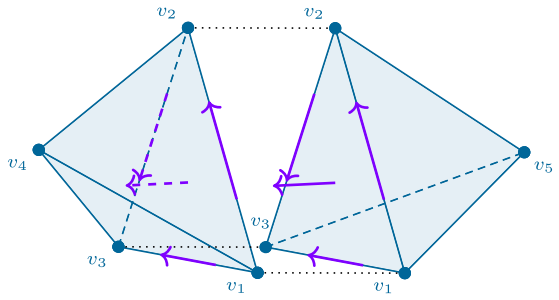

Fig. 26. Consistent orientations of neighbouring elements using vertex sequences. Edges are oriented from the lower to the higher vertex and faces according to the left-hand rule starting from the lowest vertex across the middle to the highest. As a result, the tangent and normal vectors at interfaces match.

which may be negative due to a reflection of the element in the mapping from the reference to the physical domain. The error is circumvented by taking only the absolute value of the determinant

$$\int_{V_e} \mathrm{d}V = \int_{\Omega} |\det \boldsymbol{J}| \, \mathrm{d}\Omega \,. \tag{B.6}$$

Thus, consistency is guaranteed by mapping from a single reference element.

Remark B.1. The absolute value of $\det \boldsymbol{J}$ is only used for the integration over the element. In all other use-cases, the information of the sign is necessary.

References

[1] P. Monk, Finite element methods for Maxwell's equations, Numerical Mathematics and Scientific Computation, Oxford University Press, New York, 2003, p. xiv+450, 2059447.
[2] P. Monk, An analysis of Nédélec's method for the spatial discretization of Maxwell's equations, J. Comput. Appl. Math. 47 (1) (1993) 101–121.
[3] J. Lee, D. Sun, Z. Cendes, Tangential vector finite elements for electromagnetic field computation, IEEE Trans. Magn. 27 (5) (1991) 4032–4035.
[4] P.G.S. Carvalho, P.R. Devloo, S.M. Gomes, A semi-hybrid-mixed method for Stokes–Brinkman–Darcy flows with H(div)-velocity fields, Internat. J. Numer. Methods Engrg. 125 (1) (2024) e7363.
[5] O. Duran, P.R. Devloo, S.M. Gomes, J. Villegas, A multiscale mixed finite element method applied to the simulation of two-phase flows, Comput. Methods Appl. Mech. Engrg. 383 (2021) 113870.
[6] G.A. Batistela, D. de Siqueira, P.R.B. Devloo, S.M. Gomes, A posteriori error estimator for a multiscale hybrid mixed method for Darcy's flows, Internat. J. Numer. Methods Engrg. 123 (24) (2022) 6052–6078.
[7] L. Banz, M. Ilyas, B.P. Lamichhane, W. McLean, E.P. Stephan, A mixed finite element method for the Poisson problem using a biorthogonal system with Raviart–Thomas elements, Numer. Methods Partial Differential Equations 37 (3) (2021) 2429–2445.
[8] P.E. Farrell, A. Hamdan, S.P. MacLachlan, A new mixed finite-element method for H2 elliptic problems, Comput. Math. Appl. 128 (2022) 300–319.
[9] M. Neunteufel, A.S. Pechstein, J. Schöberl, Three-field mixed finite element methods for nonlinear elasticity, Comput. Methods Appl. Mech. Engrg. 382 (2021) 113857.
[10] A.S. Pechstein, J. Schöberl, An analysis of the TDNNS method using natural norms, Numer. Math. 139 (1) (2018) 93–120.
[11] P. Neff, I.-D. Ghiba, A. Madeo, L. Placidi, G. Rosi, A unifying perspective: the relaxed linear micromorphic continuum, Contin. Mech. Thermodyn. 26 (5) (2014) 639–681.
[12] P. Neff, I.D. Ghiba, M. Lazar, A. Madeo, The relaxed linear micromorphic continuum: well-posedness of the static problem and relations to the gauge theory of dislocations, Quart. J. Mech. Appl. Math. 68 (1) (2015) 53–84.
[13] S. Owczarek, I.D. Ghiba, P. Neff, A note on local higher regularity in the dynamic linear relaxed micromorphic model, Math. Methods Appl. Sci. 44 (18) (2021) 13855–13865.
[14] N.M. Cordero, A. Gaubert, S. Forest, E.P. Busso, F. Gallerneau, S. Kruch, Size effects in generalised continuum crystal plasticity for two-phase laminates, J. Mech. Phys. Solids 58 (11) (2010) 1963–1994.
[15] F. Ebobisse, P. Neff, S. Forest, Well-posedness for the microcurl model in both single and polycrystal gradient plasticity, Int. J. Plast. 107 (2018) 1–26.
[16] L. Demkowicz, P. Monk, L. Vardapetyan, W. Rachowicz, De rham diagram for hp-finite element spaces, Comput. Math. Appl. 39 (7) (2000) 29–38.
[17] D. Pauly, M. Schomburg, Hilbert complexes with mixed boundary conditions Part 1: de Rham complex, Math. Methods Appl. Sci. 45 (5) (2022) 2465–2507.
[18] D.N. Arnold, K. Hu, Complexes from complexes, Found. Comput. Math. 21 (6) (2021) 1739–1774.
[19] D. Pauly, M. Schomburg, Hilbert complexes with mixed boundary conditions—Part 2: Elasticity complex, Math. Methods Appl. Sci. n/a (n/a).
[20] D. Pauly, W. Zulehner, The divdiv-complex and applications to biharmonic equations, Appl. Anal. 99 (9) (2020) 1579–1630.
[21] M. Botti, D.A. Di Pietro, M. Salah, A serendipity fully discrete div-div complex on polygonal meshes, C. R. Méc. (2023).
[22] J. Hu, Y. Liang, R. Ma, Conforming finite element DIVDIV complexes and the application for the linearized Einstein–Bianchi system, SIAM J. Numer. Anal. 60 (3) (2022) 1307–1330.
[23] P. Solin, K. Segeth, I. Dolezel, Higher-Order Finite Element Methods, 1st ed., Chapman and Hall/CRC, 2003.
[24] J.C. Nedelec, Mixed finite elements in $\mathbb{R}^3$, Numer. Math. 35 (3) (1980) 315–341.
[25] J.C. Nédélec, A new family of mixed finite elements in $\mathbb{R}^3$, Numer. Math. 50 (1) (1986) 57–81.
[26] F. Brezzi, J. Douglas, L.D. Marini, Two families of mixed finite elements for second order elliptic problems, Numer. Math. 47 (2) (1985) 217–235.
[27] P.A. Raviart, J.M. Thomas, A mixed finite element method for 2-nd order elliptic problems, in: I. Galligani, E. Magenes (Eds.), Mathematical Aspects of Finite Element Methods, Springer, Berlin, Heidelberg, 1977, pp. 292–315.
[28] P.G. Ciarlet, The Finite Element Method for Elliptic Problems, North-Holland Publishing Co., Amsterdam, New York, Oxford, 1978.

[29] I. Anjam, J. Valdman, Fast MATLAB assembly of FEM matrices in 2D and 3D: Edge elements, Appl. Math. Comput. 267 (2015) 252–263.
[30] A. Sky, M. Neunteufel, I. Münch, J. Schöberl, P. Neff, A hybrid $H^1 \times H(\mathrm{curl})$ finite element formulation for a relaxed micromorphic continuum model of antiplane shear, Comput. Mech. 68 (1) (2021) 1–24.
[31] A. Sky, M. Neunteufel, I. Muench, J. Schöberl, P. Neff, Primal and mixed finite element formulations for the relaxed micromorphic model, Comput. Methods Appl. Mech. Engrg. 399 (2022) 115298.
[32] A. Sky, I. Muench, P. Neff, On $[H^1]^{3\times3}$, $[H(\mathrm{curl})]^3$ and $H(\mathrm{symCurl})$ finite elements for matrix-valued curl problems, J. Eng. Math. 136 (1) (2022) 5.
[33] J. Schröder, M. Sarhil, L. Scheunemann, P. Neff, Lagrange and $H(\mathrm{curl}, \mathbb{B})$ based finite element formulations for the relaxed micromorphic model, Comput. Mech. (2022).
[34] S. Zaglmayr, High Order Finite Element Methods for Electromagnetic Field Computation (Ph.D. thesis), Johannes Kepler Universität Linz, 2006, URL https://www.numerik.math.tugraz.at/~zaglmayr/pub/szthesis.pdf.
[35] J. Schöberl, S. Zaglmayr, High order nédélec elements with local complete sequence properties, COMPEL - Int. J. Comput. Math. Electr. Electron. Eng. 24 (2) (2005) 374–384.
[36] M. Ainsworth, G. Fu, Bernstein–Bézier bases for tetrahedral finite elements, Comput. Methods Appl. Mech. Engrg. 340 (2018) 178–201.
[37] M. Ainsworth, G. Andriamaro, O. Davydov, A Bernstein–Bézier basis for arbitrary order Raviart–Thomas finite elements, Constr. Approx. 41 (1) (2015) 1–22.
[38] F. Fuentes, B. Keith, L. Demkowicz, S. Nagaraj, Orientation embedded high order shape functions for the exact sequence elements of all shapes, Comput. Math. Appl. 70 (4) (2015) 353–458.
[39] M. Ainsworth, J. Coyle, Hierarchic finite element bases on unstructured tetrahedral meshes, Internat. J. Numer. Methods Engrg. 58 (14) (2003) 2103–2130.
[40] M. El-Amrani, A. El-Kacimi, B. Khouya, M. Seaid, Bernstein-Bézier Galerkin-characteristics finite element method for convection-diffusion problems, J. Sci. Comput. 92 (2) (2022) 58.
[41] P.R.B. Devloo, C.M.A. Ayala Bravo, E.C. Rylo, Systematic and generic construction of shape functions for p-adaptive meshes of multidimensional finite elements, Comput. Methods Appl. Mech. Engrg. 198 (21) (2009) 1716–1725.
[42] D. De Siqueira, P.R. Devloo, S.M. Gomes, A new procedure for the construction of hierarchical high order hdiv and hcurl finite element spaces, J. Comput. Appl. Math. 240 (2013) 204–214, MATA 2012.
[43] F. Demore, G. Rizzi, M. Collet, P. Neff, A. Madeo, Unfolding engineering metamaterials design: Relaxed micromorphic modeling of large-scale acoustic meta-structures, J. Mech. Phys. Solids 168 (2022) 104995.
[44] L. Demkowicz, A. Buffa, H^1, $H(\mathrm{curl})$ And $H(\mathrm{div})$-conforming projection-based interpolation in three dimensions: Quasi-optimal p-interpolation estimates, Comput. Methods Appl. Mech. Engrg. 194 (2) (2005) 267–296, Selected papers from the 11th Conference on The Mathematics of Finite Elements and Applications.
[45] R. Hiptmair, D. Pauly, E. Schulz, Traces for Hilbert complexes, J. Funct. Anal. 284 (10) (2023) 109905.
[46] E. Di Nezza, G. Palatucci, E. Valdinoci, Hitchhiker's guide to the fractional Sobolev spaces, Bull. Sci. Math. 136 (5) (2012) 521–573.
[47] D. Leszek F., Lecture Notes on Energy Space, Institute for Computational Engineering and Sciences, The University of Texas at Austin, 2018, URL https://users.oden.utexas.edu/~leszek/classes/CSE393/book.pdf.
[48] M. Neunteufel, Mixed Finite Element Methods for Nonlinear Continuum Mechanics and Shells (Ph.D. thesis), Wien, 2021, URL http://hdl.handle.net/20.500.12708/17043.
[49] P. Lewintan, S. Müller, P. Neff, Korn inequalities for incompatible tensor fields in three space dimensions with conformally invariant dislocation energy, Calc. Var. Partial Differential Equations 60 (4) (2021) 150.
[50] P. Lewintan, P. Neff, Nečas–Lions lemma revisited: An L^p-version of the generalized Korn inequality for incompatible tensor fields, Math. Methods Appl. Sci. 44 (14) (2021) 11392–11403.
[51] P. Lewintan, P. Neff, L^p-Versions of generalized Korn inequalities for incompatible tensor fields in arbitrary dimensions with p-integrable exterior derivative, C. R. Math. 359 (6) (2021) 749–755.
[52] P. Neff, D. Pauly, K.J. Witsch, Poincaré meets Korn via Maxwell: Extending Korn's first inequality to incompatible tensor fields, J. Differential Equations 258 (4) (2015) 1267–1302.
[53] P. Neff, D. Pauly, K.J. Witsch, Maxwell meets Korn: A new coercive inequality for tensor fields with square-integrable exterior derivative, Math. Methods Appl. Sci. 35 (1) (2012) 65–71.
[54] F. Gmeineder, D. Spector, On Korn-Maxwell-Sobolev inequalities, J. Math. Anal. Appl. 502 (1) (2021) Id/No 125226.
[55] F. Gmeineder, P. Lewintan, P. Neff, Optimal incompatible Korn–Maxwell–Sobolev inequalities in all dimensions, Calc. Var. Partial Differential Equations 62 (2023).
[56] I.-D. Ghiba, P. Neff, A. Madeo, L. Placidi, G. Rosi, The relaxed linear micromorphic continuum: Existence, uniqueness and continuous dependence in dynamics, Math. Mech. Solids 20 (10) (2015) 1171–1197.
[57] I.-D. Ghiba, P. Neff, S. Owczarek, Existence results for non-homogeneous boundary conditions in the relaxed micromorphic model, Math. Methods Appl. Sci. 44 (2) (2021) 2040–2049.
[58] M. Ainsworth, G. Andriamaro, O. Davydov, Bernstein–Bézier finite elements of arbitrary order and optimal assembly procedures, SIAM J. Sci. Comput. 33 (6) (2011) 3087–3109.
[59] J. Gopalakrishnan, M. Neunteufel, J. Schöberl, M. Wardetzky, Analysis of curvature approximations via covariant curl and incompatibility for Regge metrics, SMAI J. Comput. Math. 9 (2023) 151–195.
[60] M. Neunteufel, J. Schöberl, Avoiding membrane locking with regge interpolation, Comput. Methods Appl. Mech. Engrg. 373 (2021) 113524.
[61] M. Neunteufel, J. Schöberl, The Hellan–Herrmann–Johnson method for nonlinear shells, Comput. Struct. 225 (2019) 106109.